ON THE EXISTENCE OF BLACK HOLES IN DISTORTED SCHWARZSCHILD SPACETIME USING MARGINALLY TRAPPED SURFACES

TERRY PILKINGTON

On the existence of black holes in distorted Schwarzschild spacetime using marginally trapped surfaces

by

© Terry Pilkington

B.Sc.

A thesis submitted to the
School of Graduate Studies
in partial fulfillment of the
requirements for the degree of
Master of Science.

Department of Physics and Physical Oceanography
Memorial University of Newfoundland

October 2010

St. John's Newfoundland

Abstract

The classical definition of a black hole in terms of an event horizon relies on global properties of the spacetime. Realistic black holes have matter distributions surrounding them, which negates the asymptotic flatness needed for an event horizon. Using the (quasi-)local concept of marginally trapped surfaces, we investigate the Schwarzschild spacetime distorted by an axisymmetric matter distribution. We determine that it is possible to locate a future outer trapping horizon for a given foliation within certain value ranges of multipole moments. Furthermore, we show that there are no marginally trapped surfaces for arbitrary values of the multipole moment magnitudes.

KEYWORDS: SCHWARZSCHILD; BLACK HOLE; DISTORTED SPACETIME; MARGINALLY TRAPPED SURFACE; FUTURE OUTER TRAPPING HORIZON

Acknowledgements

Science is a collaborative endeavour and so—except for some experimental cases—is not done in a vacuum. In that respect, there are many who deserve my thanks. First and foremost is Ivan Booth, my supervisor. Not only did Ivan provide academic guidance and insight, but was always had an open door when I felt the need to chat. Next, I would like to thank Gary Skinner who provided editing services at the low cost of my editing his project report. I am especially indebted to the following people who provided moral support throughout the process of research and writing: my parents, Mike and Pauline Pilkington; my sister, Chris Pilkington; Bonnie Russell; and Tamara Fuchinsky. Thanks also go to the new friends and collaborators I met while at Memorial University of Newfoundland.

Contents

Abstract ii

Acknowledgements iii

List of Figures vi

List of Abbreviations and Symbols viii

Introduction 1

Chapter 1. Classical Black Holes 11

1.1. Penrose-Carter Diagrams 11

1.2. Globally Defined Black Holes 13

1.3. Local Horizons 15

1.4. Weyl Solutions and the Distorted Schwarzschild Solution 18

Chapter 2. Methodology 26

2.1. The Distorted Metric & A Good Coordinate System 26

2.2. Null Normals 30

2.3. Distorting Potentials 32

Chapter 3. Results and Discussion 35

3.1. Expansion Scalars 35

3.2. Standard Foliation 36

3.3. Improved Foliation 37

3.4. Lie Derivative 39

3.5. Distorted Schwarzschild Spacetime 41

3.6. An Alternate Foliation 56

3.7. A Generic Foliation 57

3.8. Concluding Remarks 62

Appendix A. Calculations 65

A-1. Transformation from Weyl to Schwarzschild 65

A-2. Transformation from Weyl to Prolate Spheroidal 66

A-3. Transformation from Prolate Spheroidal to Schwarzschild 67

A-4. Metric Transformation Function 67

Bibliography 69

List of Figures

I Not a black hole. 1

II Comparison between Minkowski and Schwarzschild spacetimes. 6

III Kruskal-Szekeres diagram for Schwarzschild spacetime. 8

1.1 Penrose-Carter mapping. 11

1.2 Penrose-Carter diagram for Schwarzschild spacetime. 13

1.3 Penrose-Carter diagram for Minkowski spacetime. 14

1.4 Schematic of the expansion scalar. 16

1.5 Identifying the Weyl rod with the Schwarzschild event horizon. 22

3.1 Expansion scalars for the standard foliation. 37

3.2 Contour plot of the expansion scalar for a quadrupole distortion. 43

3.3 Embedding diagrams for a quadrupolarly distorted horizon. 44

3.4 Gaussian curvature of the horizon for a quadrupole distortion. 46

3.5 Contour plot of the expansion scalar for a hexadecapole distortion. 48

3.6 Embedding diagrams for a hexadecapolarly distorted horizon. 49

3.7 Gaussian curvature of the horizon for a hexadecapole distortion. 50

3.8 Contour plot of the expansion scalar for a dipole-octupole distortion. 51

3.9 Contour plot of the integrand for dipole-octupole embedding. 52

3.10 Embedding diagram for a dipole-octupole distortion. 53

3.11 Gaussian curvature of the horizon for a dipole-octupole distortion. 54

3.12 Comparison of the effects of varying α versus α_2. 55

3.13 Expansion scalars for the alternate foliation. 57

3.14 Possible trapped surfaces. 61

List of Abbreviations and Symbols

Geometric units ($G = c = 1$) will be used. The MTW sign convention $(-+++)$ will be followed for the metric. Lowercase roman indices $(a, b, c, \dots)$ will run over spacetime coordinates. The Einstein summation convention will be employed, e.g. $a_i b^i = \sum_{i=1}^{n} a_i b^i$.

Symbol	Description
v^a	A vector
ω_a	A one-form
g_{ab}	Metric tensor
$\Gamma^a_{bc} = \frac{1}{2} g^{ai} \left(g_{ib,c} + g_{ic,b} - g_{bc,i} \right)$	Christoffel symbol
$A_{a,b} = \partial_b A_a$	Partial derivative of A_a with respect to x^b
$A_{a;b} = \nabla_b A_a = \partial_b A_a - \Gamma^c_{ab} A_c$	Covariant derivative of A_a with respect to x^b
$A^a{}_{;b} = \nabla_b A^a = \partial_b A^a + \Gamma^a_{bc} A^c$	Covariant derivative of A^a with respect to x^b
q_{ab}	Induced metric on a hypersurface
$f\|_{x=n}$	The value of f evaluated at $x = n$
$d\alpha$	The exterior derivative of the form α
$\alpha \wedge \beta$	The outer-product of the forms α and β

Introduction

> Well, the thing about a black hole—its main distinguishing feature—is it's black. And the thing about space—the colour of space (your basic space colour)—is it's black. So how're you supposed to see them?
>
> Holly - *Red Dwarf*, Marooned

What is a black hole? The popular notion of a black hole as an outer-space Hoover vacuum rampaging through the Universe, sucking up everything—including light—is inaccurate at best. This misconception stems from the fact that there indeed exists a region surrounding the black hole from which not even light can escape. The perceived size of this region is, however, greatly overestimated. The "no escape" region extends only a distance of approximately 3 $\frac{\text{km}}{\text{M}_\odot}$ from the centre of the object (that is: the radius of the region is approximately three kilometres per solar mass.) Even with this region, the gravitational influence of a black hole is the same

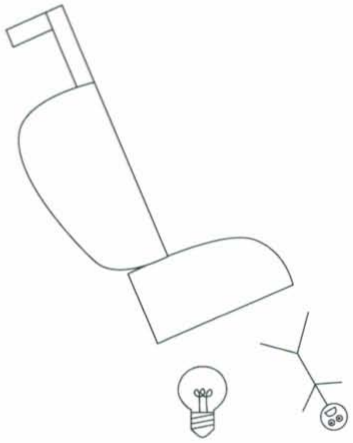

FIGURE I. Not a black hole.

as any other massive object. Were we to replace our sun with a black hole of the same mass, the "no escape" region would only be 6 km wide and there would be virtually no difference in the orbit of any body in the solar system.

The idea of such an object is not a new one. In 1784, working from Newton's ideas of gravitation and corpuscular light, John Michell published a letter, [**1**], in which he describes a method for finding the distance and brightness of a star. In this letter, he speculates on "a sphere of the same density with the sun [whose mass] were to exceed that of the sun in proportion of 500 to 1... [and] supposing light to be attracted by the same force in proportion to its vis inertiæ... all light emitted from such a body would be made to return towards it, by its own proper gravity." An object could be so massive and of such a size that its escape velocity is greater than the speed of light.

This same idea—an object from which light could not escape—was also discussed by Laplace in the first two editions of his *Exposition du Système du Monde*. However, he removed it from later editions as the wave theory of light took over from the corpuscular theory [**2, 3**]; a light wave would have no mass and could therefore not be affected by gravity.

The idea was revived by Anderson in 1920 and Lodge in 1921 [**2**]. Both speculated on objects of sufficient density and size such that their escape velocity would meet or exceed the speed of light. Lodge goes on to discount the solar-sized dark objects on the basis that an object that small could not have the requisite density. On the other hand, he accepts the possibility of dark objects the size of a galaxy.

Mathematically, objects that we would recognize as black holes originate with the Schwarzschild solution to Einstein's field equations in general relativity. The field equations relate the curvature of spacetime (the Ricci tensor) to the matter and energy present (the stress-energy tensor) in the spacetime. A common form of these

equations would be (see, e.g., [**4**])

$$R_{ab} - \frac{1}{2} g_{ab} \mathcal{R} = 8\pi T_{ab}$$

where R_{ab} is the Ricci tensor, $\mathcal{R} = g^{ab} R_{ab}$ is the Ricci scalar, g_{ab} is the metric tensor and T_{ab} is the stress-energy tensor. Since R_{ab} involves combinations of the metric and its derivatives, Einstein's equations are then a complicated set of non-linear partial differential equations with the metric as the solution.

There are many solutions to the field equations, probably the simplest of these being Minkowski's (flat) spacetime. The flat metric is given—in the usual spherical polar coordinates—by the line element

$$ds^2 = g_{ab}\, dx^a\, dx^b = -dt^2 + dr^2 + r^2 d\theta^2 + r^2 \sin^2\theta\, d\phi^2.$$

This metric has $R_{ab} = 0$—no curvature, flat—and $T_{ab} = 0$—empty, vacuum.

The Schwarzschild solution, named for Karl Schwarzschild who first derived it in 1916, describes the empty exterior portion of a static, spherically symmetric mass. The metric is given by

$$ds^2 = -\left(1 - \frac{2m}{r}\right) dt^2 + \frac{dr^2}{1 - \frac{2m}{r}} + r^2 d\theta^2 + r^2 \sin^2\theta\, d\phi^2$$

where m is the mass of the object and $(t,\ r,\ \theta,\ \phi)$ are the Schwarzschild coordinates, similar to spherical polar coordinates. Not only is this *a* solution for static, spherically symmetric spacetimes, but Birkhoff showed that it is *the only* solution for spherically symmetric spacetimes and Israel showed that if the spacetime is static, then it *must* be Schwarzschild [**5**].

It might not be immediately obvious that this solution necessarily describes a black hole. Indeed, it was not until the 1950s that it was recognized as such, and not

until the 1960s that the idea of black holes as real objects was accepted. Notice that the Schwarzschild solution has two singularities: $r = 0$ and $r = 2m$. The singularity at the origin, $r = 0$, is a true singularity and it describes a breakdown of the spacetime. At $r = 2m$, however, there is simply a breakdown of the coordinate system. If an observer were to travel from, say, $r = 3m$ to $r = m$, they would notice no ill effects upon crossing $r = 2m$ beyond the usual tidal effects (which may be rather painful depending on m.) They would find, to their dismay, that they could not return to their original position—nor could they go outward beyond $r = 2m$—without somehow exceeding the speed of light.

Though it is only a coordinate singularity, the spacetime at $r = 2m$ is of some interest and is given the name of the Schwarzschild radius or the Schwarzschild singularity. For all spatial points defined by the Schwarzschild radius—the set

$$\mathcal{H}_t = \Big\{(2m,\, \theta,\, \phi) \mid 0 \leq \theta < \pi,\, 0 \leq \phi < 2\pi\Big\}$$

—we have, at any time t, a spherical surface, $\mathcal{H}_t$, called the Schwarzschild surface. This surface separates the "normal" spacetime from the "odd" region $r < 2m$. In more modern terminology, the Schwarzschild surface is called the event horizon, a term coined by Rindler in the 1950s [**3**].

At the time of his solution, Schwarzschild viewed the surface which bears his name as a physical barrier and a true singularity [**2**]. He calculated that a body could not be compressed to less than $r = \frac{9}{8}(2m)$ [**6**], so compressing to $r = 2m$ would not be possible, indeed unphysical and safely hidden away deep inside real bodies. This view was shared by many, including Einstein [**3**] and Eddington who called the Schwarzschild radius a "magic circle which no measurement can bring us inside" [**2**].

Despite these misgivings, it was shown multiple times that the Schwarzschild metric truly is non-singular at $r = 2m$. Panlevé, 1921, and Gullstrand, 1922, obtained a coordinate transformation such that the metric took the form [**5**]

$$ds^2 = -dT^2 + \left(dr + \sqrt{\frac{2m}{r}}dT\right)^2 + r^2 d\theta^2 + r^2 \sin^2\theta \, d\phi^2.$$

Eddington, 1924, and Finkelstein, 1958, obtained [**5**]

$$ds^2 = -\left(1 - \frac{2m}{r}\right) dv^2 + 2dv\, dr + r^2 d\theta^2 + r^2 \sin^2\theta \, d\phi^2.$$

Kruskal, 1950s, and Szekeres, 1960, had [**5**]

$$ds^2 = -\frac{32m^3}{r} e^{-\frac{r}{2m}} dU\, dV + r^2 d\theta^2 + r^2 \sin^2\theta \, d\phi^2.$$

Each of these is clearly non-singular at $r = 2m$. It seems odd that Eddington was able to find a non-singular version of the metric, yet utter the quote above. This is most likely due to the view of the incompressibility of matter—i.e. the $r \geq \frac{9}{8}(2m)$ limit that Schwarzschild calculated—which was slowly crumbling away.

Oppenheimer and Snyder showed [**7**] that infinite gravitational collapse can not only occur, but it would occur in finite time (for a solar mass star, complete collapse would take about a day.) Roughly speaking, once the star's core has stopped burning its nuclear fuel, gravity will quickly overcome the outward light pressure that had been present but would now fade away, causing collapse. The general acceptance of the whole Schwarzschild spacetime (and not just the exterior region) as an object for study was not achieved until the 1960s. The term that we use today to describe these objects, "black holes," was not introduced until 1967. Wheeler, who was tired of calling them "gravitationally completely collapsed objects", was giving a talk in 1967

where he solicited the crowd for a better term [**8**]. He liked the shouted suggestion, due to the conceptual connection to a black body, and used it at every opportunity.

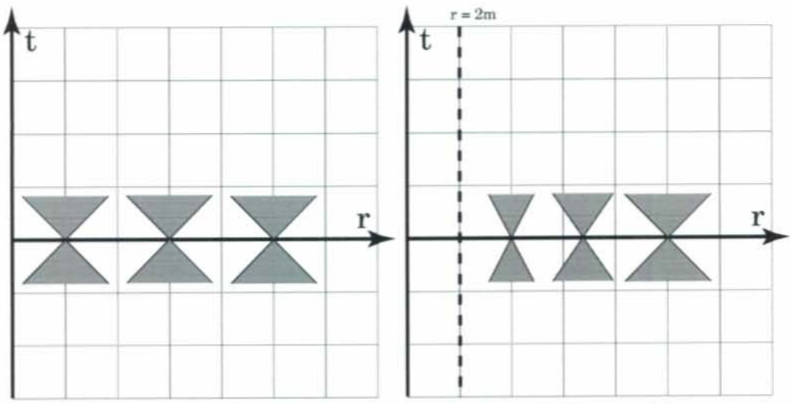

(A) Minkowski (B) Schwarzschild

FIGURE II. Comparison between Minkowski and Schwarzschild spacetimes.

A convenient conceptual way of exploring spacetime is through the use of spacetime diagrams. We can see two examples in Figure IIa and Figure IIb, where we compare flat spacetime to Schwarzschild spacetime. Both have time on the vertical axis and radial distance on the horizontal (the angular dimensions have been suppressed.) To be able to see the structure of a spacetime we use light cones, which are displayed as shaded regions on the diagrams. Light cones are formed by the paths of ingoing and outgoing light rays—called null curves—through a point in spacetime. For flat spacetimes,

$$0 = -dt^2 + dr^2 \qquad \Longrightarrow \qquad \frac{dt}{dr} = \pm 1.$$

So, light cones have slope ± 1 (the speed of light) in flat spacetimes. The paths of massive objects will necessarily travel inside of some light cone at each point in the spacetime. For Schwarzschild,

$$0 = -\left(1 - \frac{2m}{r}\right) dt^2 + \frac{dr^2}{1 - \frac{2m}{r}} \qquad \Longrightarrow \qquad \frac{dt}{dr} = \pm \frac{1}{1 - \frac{2m}{r}}.$$

Perhaps surprisingly, the light cones in Schwarzschild depend on the distance from the black hole. As $r \to \infty$, the slopes of the light cones approach ± 1, and so the spacetime becomes flat far from the source. But, as $r \to 2m$, the slopes become infinite; as seen in Figure IIb, the lightcones close up.

As we've already noted, this is an artifact of the coordinate system, so we can choose a different system to investigate the whole spacetime. While spacetime diagrams can be constructed for Panlevé-Gullstrand and Eddington-Finkelstein coordinates, the most instructive for our purposes is the Kruskal-Szekeres spacetime diagram, shown in Figure III. The benefits of the Kruskal-Szekeres coordinates are twofold. First, U and V are null coordinates. Notice that lightcones occur along $U =$ const. and $V =$ const., i.e. along lines of slope ± 1.

Secondly, the Kruskal-Szekeres solution is a maximally extended Schwarzschild solution. There are no restrictions on the values of U or V and so we end up with mirror images of the usual Schwarzschild spacetime. There are two exterior and two interior regions. The usual Schwarzschild solution is contained in regions I and II. Regions III and IV mirror I and II respectively. The location to which we usually ascribe the event horizon occurs for $V = 0$, $U \geq 0$ and we end up with three additional horizons.

The Kruskal-Szekeres diagrams are useful tools in examining the structure of a spacetime, but there is one further tool we will need to be able to present the modern

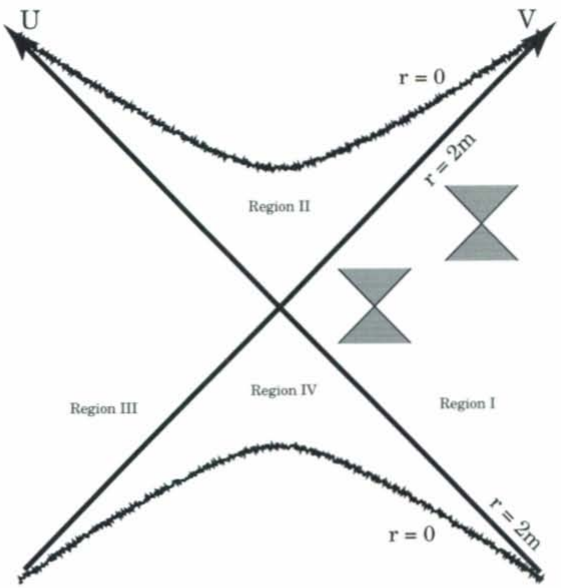

FIGURE III. Kruskal-Szekeres diagram for Schwarzschild spacetime.

mathematical definition of a black hole. This tool, called the Penrose-Carter diagram, and the mathematical definition it illuminates will be presented in the following chapter along with its associated problems. Unlike the furor over the Schwarzschild singularity, the problems with the modern definition are subtle but no less fundamental—in a sense more to do with semantics than just a poor choice of coordinates.

The solution obtained by Schwarzschild and extended by others is a highly idealized solution. To calculate the solution, Schwarzschild had to impose strict symmetries that, while easing calculations, meant the spacetime described by his solution is not a terribly realistic one. This is not such a great problem; in all areas of physics,

we must make restrictive assumptions to obtain a first approximation. A more realistic solution—a next approximation—would not contain all of the symmetries of the original solution, but would more accurately describe a physical black hole.

Furthermore, the event horizon is a global object. As we will see below, a black hole is defined by an event horizon. That is, it relies on properties of the entire spacetime rather than just the properties of the black hole itself. A more realistic black hole may not have the appropriate global structure and cannot then be modelled by a spacetime with an event horizon. We would like, then, a definition of a black hole in terms quasi-local to the black hole. We use the distinction quasi since they depend on surfaces rather than a single point. For the remainder, we will take local to actually mean quasi-local. Different candidates exist for such a local definition which all rely on the notion of trapped surfaces. Trapped surfaces depend only on the local structure of a spacetime; the structure near the black hole. The idea of using trapped surfaces to locate black holes predates the use of event horizons. Penrose [**9**] used them to show that a singularity must form in gravitational collapse like that described by Oppenheimer and Snyder. The event horizon replacement we will use is the future outer trapping horizon. These are described by marginally trapped surfaces, which are a limiting case of trapped surfaces.

For the purposes of this monograph, we will be interested in Schwarzschild solutions that have been distorted by the presence of axisymmetric matter distributions. It is not entirely clear whether they remain black holes. The classical definition discussed in the next chapter is of little use. Since the distortions destroy asymptotic flatness in vacuum, we cannot in fact use such a definition. In that respect, we ask the question: Do arbitrary distorted Schwarzschild spacetimes always contain a trapping horizon? In other words: Are marginally trapped surfaces an appropriate framework

for describing distorted Schwarzschild black holes? These questions will be answered thus: We will check whether a set of distorted Schwarzschild solutions are indeed black holes by looking for marginally trapped surfaces.

This monograph will be structured as follows. The first chapter will discuss the mathematical framework of black holes, its problems and their solutions. The second chapter will contain the methodology and some general results of distorted Schwarzschild spacetimes. The final chapter will discuss specific results. Lengthy calculations and results will be relegated to appendices.

CHAPTER 1

Classical Black Holes

Once it had been decided that gravitational collapse could occur and that the Schwarzschild "singularity" was nothing more than a coordinate singularity, a fruitful period of research into black holes occurred. From the uniqueness theorems to the laws of black hole mechanics which describe black holes as thermodynamic systems complete with a temperature and entropy, the 1960s and 1970s were a busy time for mathematical physicists. A powerful tool involved in this research was the Penrose-Carter diagram.

1.1. Penrose-Carter Diagrams

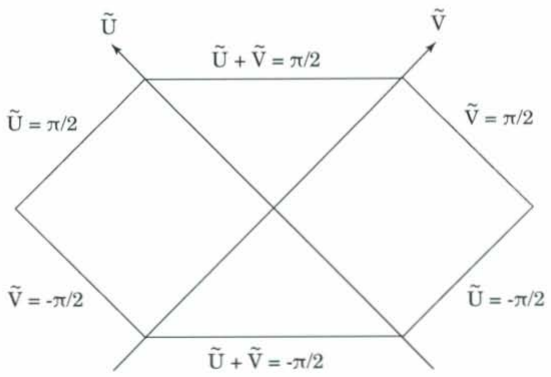

FIGURE 1.1. Penrose-Carter mapping.

Penrose-Carter diagrams (also called conformal diagrams) are spacetime diagrams that contain the whole of the spacetime. For each of the spacetime diagrams discussed in the Introduction, $t \to \pm\infty$ or $r \to \infty$ is well off the page. To be able to examine the whole of the spacetime on a single finite diagram, we compactify the spacetime by performing the transformations [**5**]

$$\tilde{U} = \arctan U \qquad \text{and} \qquad \tilde{V} = \arctan V,$$

where U and V are the Kruskal-Szekeres coordinates from the Introduction. With this transformation, we obtain the spacetime diagram shown in Figure 1.1 and we can make the following identifications.

The surfaces $\tilde{U} = \frac{\pi}{2}$ and $\tilde{V} = \frac{\pi}{2}$ contain the end points of all outgoing null rays. We call these surfaces future null infinity and denote them by the symbol $\mathscr{I}^+$. Similarly, the surfaces $\tilde{U} = -\frac{\pi}{2}$ and $\tilde{V} = -\frac{\pi}{2}$ are called past null infinity and symbolized by $\mathscr{I}^-$. The points where $\mathscr{I}^+$ meets $\mathscr{I}^-$ are spacelike infinity ($r = \infty$) labelled by i^0. The points $r = 0$ becomes the surfaces $\tilde{U} + \tilde{V} = \pm\frac{\pi}{2}$ and $r = 2m$ stays at $\tilde{U} = U = 0$ and $\tilde{V} = V = 0$, showing both singularities and both horizons present in the maximally extended Schwarzschild solution. The points $(\tilde{U}, \tilde{V}) = \left(0, \frac{\pi}{2}\right)$ and $(\tilde{U}, \tilde{V}) = \left(\frac{\pi}{2}, 0\right)$ are called future timelike infinity, which represent any point $t = \infty$ and r finite, labelled by i^+. Similarly, i^- represents $t = -\infty$, r finite, thus the points $(\tilde{U}, \tilde{V}) = \left(0, -\frac{\pi}{2}\right)$ and $(\tilde{U}, \tilde{V}) = \left(-\frac{\pi}{2}, 0\right)$. The fully labelled Penrose-Carter diagram for Schwarzschild spacetime is shown in Figure 1.2.

These diagrams allow for a map of the whole causal structure of a spacetime. The mapping from Kruskal-Szekeres coordinates is conformal, which means angle preserving, so the light cones still have slope ± 1. How can we use this to define a black hole? To answer this, we need one final piece of notation.

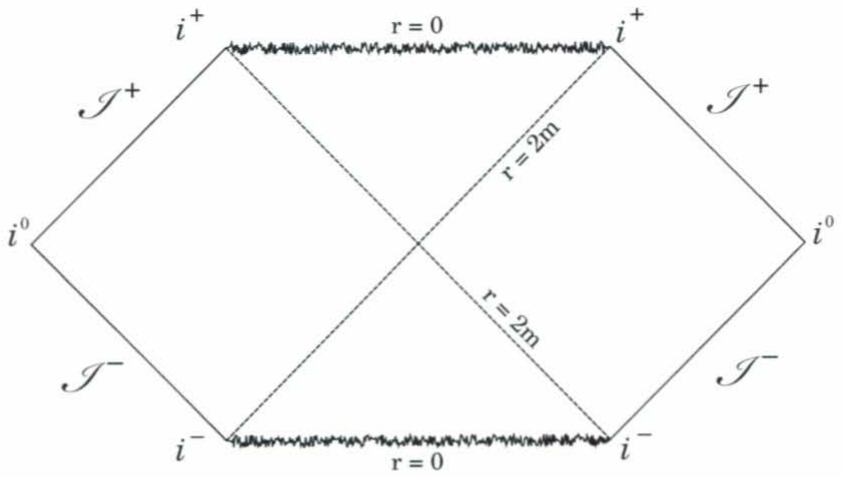

FIGURE 1.2. Penrose-Carter diagram for Schwarzschild spacetime.

1.2. Globally Defined Black Holes

Consider an event p. Then, all future directed (timelike or null) curves from p are denoted by the set $J^+(p)$, called the causal future of p. Similarly, the causal past of p, $J^-(p)$, would be the set of all past-directed curves from p. We can extend this to a whole set of events, $S = \{p_i\}$, in that $J^+(S) = \bigcup_{p\in S} J^+(p)$ and $J^-(S) = \bigcup_{p\in S} J^-(p)$. We can now define [**4**] a black hole, $\mathcal{B}$, in a manifold, $\mathcal{M}$, as

$$\mathcal{B} = \mathcal{M} - J^-\left(\mathscr{I}^+\right), \tag{1.1}$$

the region in a manifold without the causal past of future null infinity. If $\mathcal{B}$ is non-empty, then it is said that there exists a black hole in the spacetime. The boundary of the black hole region is then the event horizon,

$$\mathcal{H} = \partial\mathcal{B} = \dot{J}^-\left(\mathscr{I}^+\right). \tag{1.2}$$

Equation 1.1 is the mathematical statement of "no light can escape a black hole." We thus defined a black hole by locating an event horizon in a spacetime. Furthermore, we can determine this existence graphically using a Penrose-Carter diagram. If we compare the Penrose-Carter diagram of Minkowski spacetime, Figure 1.3, to that of Schwarzschild spacetime, Figure 1.2, it is quite obvious which spacetime contains a black hole. In Minkowski spacetime, we see that $J^-(\mathscr{I}^+)$ covers the entire spacetime and so $\mathcal{B}$ is empty.

The definition of a black hole in terms of the causal structure of spacetime was established by Hawking & Ellis [**10**], and it provided the foundation for the achievements mentioned at the beginning of this chapter. There are, unfortunately, problems in defining black holes this way. The inclusion of $\mathscr{I}^+$ means that we have to trace all null curves to determine the presence of a black hole. The event horizon is thus defined by boundary conditions infinitely far away. Hayward remarks, [**11**], that "the location of the event horizon, or even its existence, is known only after the universe has ended, or, depending on one's religious beliefs, to the gods looking down on space-time as a vast Penrose diagram."

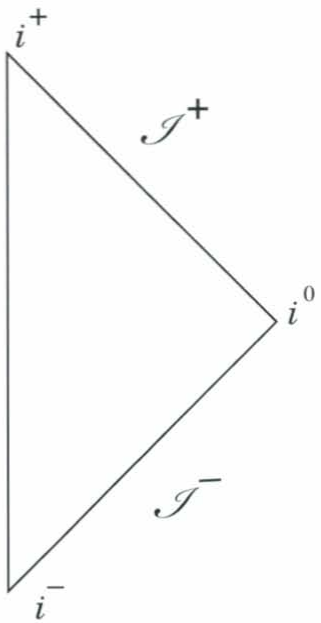

FIGURE 1.3. Penrose-Carter diagram for Minkowski spacetime.

Notice also that the definition in Equation 1.1 makes no mention of strong gravitational fields or local aspects of a black hole. Furthermore, the event horizon seems to be aware of its own future. For example, [**12**], an event horizon can form in a flat region of Vaidya spacetime (i.e. no gravitational field at all) in anticipation of future collapse. As another example (see, e.g., [**13**]), in the collapse of two matter shells in Vaidya spacetime the event horizon formed by the first shell will start to expand before the second shell reaches it and stops expanding when the last of the second shell crosses the location of the new horizon. While the global definitions of a black hole provides many powerful and useful results, it also gives some strange results. A new definition is thus desired.

1.3. Local Horizons

The use of a local definition to replace the notion of an event horizon was first put forth by Hájiček in 1973 [**14**], and promoted by Hayward [**15**] and Ashtekar, Beetle & Fairhurst [**16**]. All of these definitions start from the concept of trapped surfaces, but before we can discuss trapped surfaces, we must first introduce the expansion scalar.

The optical scalars (the expansion, θ; shear, σ; and rotation, ω) were originally introduced by Sachs who was investigating gravitational waves [**17**]. He needed a way to determine how the image of an object would be altered as it travelled along a null geodesic. The current definitions of the optical scalars are in terms of a congruence of null geodesics.

First, consider a spacelike 2-surface, S, as in Figure 1.4. Then pass (non-intersecting) null geodesics through each point in S, this set of geodesics is the congruence. Now travel a fixed distance, ϵ, along each of the geodesics. This defines a new 2-surface

S'. Thus, the expansion can be written as

$$\Theta = \lim_{\epsilon \to 0} \frac{1}{\epsilon} \frac{\delta A' - \delta A}{\delta A}, \tag{1.3}$$

the change in the area element around each point in the surface along the congruence.

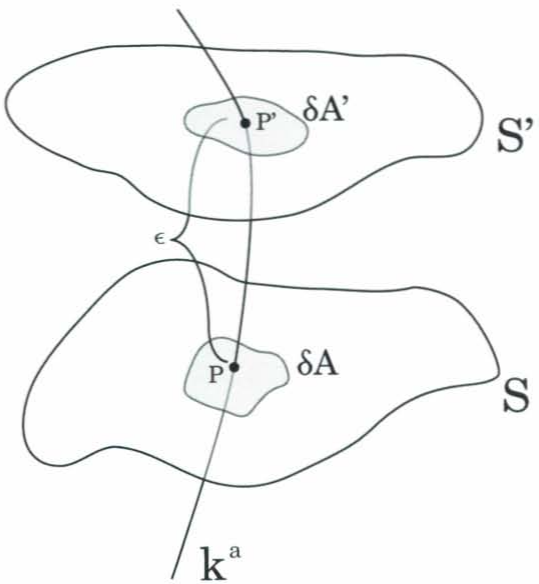

FIGURE 1.4. Schematic of the expansion scalar, $\Theta_{(k)}$

Alternatively, we can consider a vector field, k^a, tangent to the congruence. This vector field will be null, $k^a k_a = 0$, and affinely parameterized, $k^a_{;b} k^b = 0$ (where the semicolon represent covariant differentiation with respect to the full spacetime metric.) We introduce another null vector, N^a, such that $k_a N^a = -1$. Then the

induced metric on S is given by

$$q_{ab} = g_{ab} + k_a N_b + N_a k_b \tag{1.4}$$

where g_{ab} is the full spacetime metric. The induced metric satisfies $q_{ab}k^b = q_{ab}N^b = 0$, $q^a_{\ b}q^{bc} = q^{ac}$ and $q^a_{\ a} = 2$. Notice that the conditions on the auxiliary null vector do not uniquely determine N_a. However, Θ does not depend on the choice of N^a, and so Θ is unique.

Using the induced metric, q_{ab}, and the tangent vector, k^a, we can define the expansion scalar as

$$\Theta_{(k)} = q^{ab}k_{a;b}. \tag{1.5}$$

The evolution of the expansion scalar is determined by Raychaudhuri's equation. If k^a is affinely parameterized by λ, then [**5**]

$$\frac{d\Theta_{(k)}}{d\lambda} = -\frac{1}{2}\Theta^2_{(k)} - \sigma_{ab}\sigma^{ab} + \omega_{ab}\omega^{ab} - R_{ab}k^a k^b$$

where σ_{ab} is the shear tensor and ω_{ab} is the rotation tensor and they are the tensorial extensions of the scalars introduced by Sachs. If the congruence is hypersurface orthogonal, $\omega_{ab} = 0$, and if the null energy condition holds, $R_{ab}k^a k^b \leq 0$. Then,

$$\frac{d\Theta_{(k)}}{d\lambda} = -\frac{1}{2}\Theta^2_{(k)} - \sigma_{ab}\sigma^{ab} - R_{ab}k^a k^b \leq 0.$$

This implies that if a congruence of geodesics starts to converge, then they must meet at some point in the future.

We can now define trapped surfaces in the following manner. Consider a closed, spacelike 2-surface, Σ, embedded in a spacetime, $(\mathcal{M}, g)$. There are then two future-directed null one-forms, ℓ_a and n_a, normal to Σ with associated expansions $\Theta_{(\ell)}$ and

$\Theta_{(n)}$. We associate ℓ_a with the outward direction and n_a the inward. If $\Theta_{(\ell)} < 0$ and $\Theta_{(n)} < 0$, then Σ is said to be a trapped surface. If $\Theta_{(\ell)} = 0$ and $\Theta_{(n)} < 0$, then Σ is said to be a marginally trapped surface. It is these marginally trapped surfaces which we will use to determine the existence of black holes in distorted Schwarzschild spacetime.

The main candidates for replacing the event horizon to define a black hole all start from trapped surfaces. For reviews of the various local horizons, the interested reader is directed to [**13**]. Here, we will concentrate on future outer trapping horizons (FOTHs). A FOTH is defined [**11**] as a hypersurface, $\mathcal{H} = \bigcup_{t\in\mathbb{R}} S_t$, of a spacetime, $(\mathcal{M}, g)$, which satisfies

i. $\Theta_{(\ell)} = 0$ and $\Theta_{(n)} < 0$; and

ii. $\mathcal{L}_n\Theta_{(\ell)} < 0$.

That is, a FOTH is foliated by marginally trapped surfaces, S_t, and, just inside the horizon, the outward null geodesics are also converging.

The use of a FOTH provides a local definition of a black hole that we desire in general and which we require for distorted spacetimes in particular. It is obviously associated with strong gravitational fields since, in regions of weak fields, $\Theta_{(\ell)} > 0$, and so no trapped surfaces are present (be they marginally or fully trapped.) Furthermore, trapped surfaces in a spacetime imply the existence of a singularity as shown first by Penrose [**9**].

1.4. Weyl Solutions and the Distorted Schwarzschild Solution

As described in the beginning of this chapter, the usual definition of a black hole involves $\mathscr{I}^+$. Thus, we need a spacetime with the appropriate conformal structure at infinity: the spacetime must be asymptotically flat. There are many different

definitions of asymptotic flatness, which are all roughly equivalent in vacuum. A working definition which we find instructive is that a spacetime is asymptotically flat if it approaches flat (Minkowski) spacetime at infinity. The technical details of this can be seen in, for example, [**4**] or [**18**]. The requirement of asymptotic flatness in defining an event horizon (and thus a black hole) is not completely arbitrary. Due to the non-linear nature of Einstein's field equations, we must make restrictive assumptions. Among these assumptions, that the black hole is isolated figures prominently. This approximation gave us a wealth of knowledge about the properties of black holes. We would like now to move on to the next approximation; a more realistic model of a black hole. Paraphrasing Chandrasekhar, [**19**], if we assume some external distribution of matter, what we are really doing is relaxing the assumption of asymptotic flatness. How then do we relax this assumption?

The effects of an external field (that is, some distribution of matter) on the Schwarzschild spacetime was investigated on two fronts through the 1960s and 1970s. A perturbative approach was undertaken by Regge & Wheeler [**20**], Zerilli [**21**] and Vishveshwara [**22**]. This approach took a known solution (e.g. Schwarzschild) and added perturbations. It continues to the present day; see, e.g., [**23**] for a gauge-invariant formulation. The outcome of these investigations was that the Schwarzschild spacetime is stable against small perturbations. Thus, Schwarzschild black holes can exist in more realistic situations. This approach kept the geometry of the original known solution; the perturbations are small and linear. The other approach was to distort the metric itself, resulting in a new spacetime with new geometric properties.

Mysak and Szekeres asked if the Schwarzschild surface at $r = 2m$ was affected by a general, exterior, static field in terms of a polynomial expansion [**24**]. They found that this type of distortion had no effect on the surface. However, time-dependent

distortions caused the Schwarzschild surface to become a true singularity. Israel and Khan were investigating the interaction of multiple Schwarzschild "particles" (not yet called black holes) [**25**]. They found that, for regular distortions, the Schwarzschild surface remained regular and no new singularities appeared. In the course of investigating non-spherical gravitational collapse Doroshkevich, Zel'dovich and Novikov showed that, for an external quadrupole field, the Schwarzschild surface remains regular [**26**]. In response to Bekenstein's conjecture (later proved by Hawking) that a black hole's entropy is related to its area, Israel found that the event horizon was tidally deformed by a static axisymmetric matter distribution, but remained regular [**27**]. However, there is no mention of asymptotic flatness with regards to the matter distribution, so his use of "event horizon" is likely a matter of convention rather than an actual event horizon.

The approach of distorting the metric begins by using a special class of solutions known as the Weyl metric. For a static, axisymmetric, vacuum spacetime, the metric takes the form [**28**]

$$ds^2 = -\mathrm{e}^{2\psi}dt^2 + \mathrm{e}^{2(\gamma-\psi)}\left(d\rho^2 + dz^2\right) + \mathrm{e}^{-2\psi}\rho^2 d\phi^2 \tag{1.6}$$

in Weyl canonical coordinates $(t,\ \rho,\ z, \phi)$, where $\psi \equiv \psi(\rho, z)$ and $\gamma \equiv \gamma(\rho, z)$. This metric contains all static, axisymmetric solutions to Einstein's field equations. Specific spacetimes are defined by the choice of ψ and γ. In view of a distorted spacetime, we can think of it in two different ways. The first is that the spacetime remains vacuum, in which case the distortions are implicit in the metric. The other method is to consider the distortions to be caused by the presence of external matter. For example, one could use spacetime-surgery techniques to replace the asymptotic region of Equation 1.6 with an asymptotically flat spacetime such as the usual Schwarzschild

solution. The matter distribution at the junction of the spacetimes can then be viewed as inducing the distortion. For the Weyl metric, the field equations reduce to a set of three equations: one for ψ and two for γ. The equation for ψ is given by [**29**]

$$\frac{\partial^2\psi}{\partial\rho^2} + \frac{1}{\rho}\frac{\partial\psi}{\partial\rho} + \frac{\partial^2\psi}{\partial z^2} = 0. \tag{1.7}$$

If we consider an unphysical three dimensional Euclidean space, Σ, defined by the line element

$$d\sigma^2 = d\rho^2 + \rho^2 d\phi^2 + dz^2$$

then Equation 1.7 is simply the Laplacian of ψ in Σ. Recall that the Laplacian is linear (i.e. if ψ_1 and ψ_2 are each solutions to the Laplacian, then so is $\psi = \psi_1 + \psi_2$.) Once we have determined ψ, the other function, γ, can be calculated from the remaining field equations

$$\frac{\partial\gamma}{\partial\rho} = \rho\left[\left(\frac{\partial\psi}{\partial\rho}\right)^2 - \left(\frac{\partial\psi}{\partial z}\right)^2\right] \qquad \text{and} \qquad \frac{\partial\gamma}{\partial z} = 2\rho\frac{\partial\psi}{\partial\rho}\frac{\partial\psi}{\partial z}. \tag{1.8}$$

When considering the vacuum version of the Weyl metric, we check the Ricci tensor. Recall that the Ricci tensor is given by contraction of the Riemann tensor,

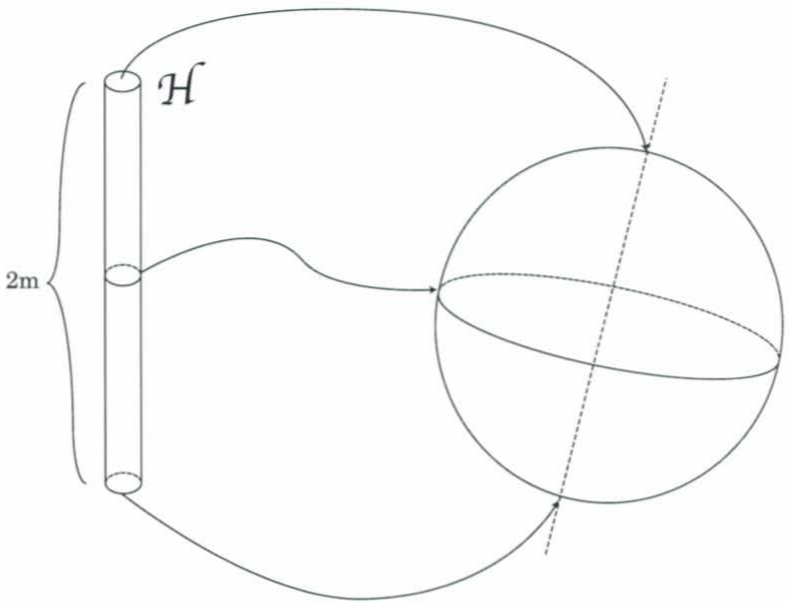

FIGURE 1.5. Identifying the Weyl rod with the Schwarzschild event horizon. Diagram adapted from [**30**]

$R_{ab} = g^{cd}R_{acbd}$. In Weyl canonical coordinates, we get

$$R_{tt} = \mathrm{e}^{-2\gamma+4\psi}\left[\frac{\partial^2\psi}{\partial\rho^2} + \frac{1}{\rho}\frac{\partial\psi}{\partial\rho} + \frac{\partial\psi}{\partial z}\right]$$

$$R_{\rho\rho} = \frac{\partial^2\psi}{\partial\rho^2} + \frac{1}{\rho}\frac{\partial\psi}{\partial\rho} + \frac{\partial\psi}{\partial z} - 2\left(\frac{\partial\psi}{\partial\rho}\right)^2 - \left[\frac{\partial^2\gamma}{\partial\rho^2} - \frac{1}{\rho}\frac{\partial\gamma}{\partial\rho} + \frac{\partial^2\gamma}{\partial z^2}\right]$$

$$R_{\rho z} = R_{z\rho} = \frac{1}{\rho}\frac{\partial\gamma}{\partial z} - 2\frac{\partial\psi}{\partial\rho}\frac{\partial\psi}{\partial z}$$

$$R_{zz} = \frac{\partial^2\psi}{\partial\rho^2} + \frac{1}{\rho}\frac{\partial\psi}{\partial\rho} + \frac{\partial\psi}{\partial z} - 2\left(\frac{\partial\psi}{\partial z}\right)^2 - \left[\frac{\partial^2\gamma}{\partial\rho^2} + \frac{1}{\rho}\frac{\partial\gamma}{\partial\rho} + \frac{\partial^2\gamma}{\partial z^2}\right]$$

$$R_{\phi\phi} = \mathrm{e}^{-2\gamma}\rho^2\left[\frac{\partial^2\psi}{\partial\rho^2} + \frac{1}{\rho}\frac{\partial\psi}{\partial\rho} + \frac{\partial\psi}{\partial z}\right]$$

where all other entries are zero. Now, using the field equations—Equation 1.7 and Equation 1.8—the Ricci tensor becomes

$$R_{ab} = 0 \tag{1.9}$$

as expected. The distorted Weyl metric represents vacuum spacetimes.

For normal, undistorted Schwarzschild spacetime, we have [**28**]

$$\psi_S = \frac{1}{2}\ln\left(\frac{r_+ + r_- - 2m}{r_+ + r_- + 2m}\right) \qquad \gamma_S = \frac{1}{2}\ln\left(\frac{(r_+ + r_-)^2 - 4m^2}{4r_+ r_-}\right)$$

where $r_\pm^2 = \rho^2 + (z \pm m)^2$. Furthermore, ψ_S is simply the flat space Newtonian potential of a rod, $\mathcal{H}$, of length $2m$ and mass m placed symmetrically on the $\rho = 0$ axis [**29**]. This rod can be mapped to the Schwarzschild event horizon by identifying the ends of the rod with the poles of the horizon and the middle of the rod with the equator of the horizon as in Figure 1.5. The rod is, of course, only one-dimensional.

We can consider a distortion as an addition to the potential ψ_S. Since Equation 1.7 is linear in ψ, we let

$$\psi = \psi_S + U \tag{1.10}$$

and, though the equations for γ are not linear, it is helpful to consider the same form for γ,

$$\gamma = \gamma_S + V$$

where ψ_S and γ_S are the functions given earlier for the normal, undistorted Schwarzschild spacetime. We then associate the functions $U \equiv U(\rho, z)$ and $V \equiv V(\rho, z)$ with the distortion. If there is no distortion (i.e. $U = V = 0$), then $\psi = \psi_S$ and $\gamma = \gamma_S$, which is the undistorted Schwarzschild spacetime as expected. We can also consider the

distortion alone: let $\psi_S = \gamma_S = 0$, then $\psi = U$ and $\gamma = V$. Thus, we can regard the distorted Weyl metric as a Schwarzschild black hole in some background spacetime.

From Geroch & Hartle [**31**] and Fairhurst & Krishnan [**29**], we get restrictions on U. The first is that U must take the same value, u_0, at both ends of $\mathcal{H}$ (i.e. both poles.) This is so that V vanishes on the $\rho = 0$ axis (i.e. the location of the horizon will not be affected.) Furthermore, on the horizon,

$$2U - V = 2u_0. \tag{1.11}$$

The two different viewpoints introduced after the Weyl metric, Equation 1.6, lead to restrictions on u_0. Recall that the first is that the spacetime remains vacuum. However, since U satisfies Equation 1.7, it will diverge at infinity. This means that Equation 1.6 will not approach Minkowski—asymptotic flatness is destroyed. Then, we must consider all values of u_0. As Geroch & Hartle point out, the Weyl solutions have vanishing stress-energy and so the distorting matter is not explicitly seen in Einstein's equations. To this end, we can consider that our Weyl solution represents only a neighbourhood of the horizon. That is, U only satisfies the vacuum field equations (Equation 1.7) near the horizon and we must extend U and V such that they tend to zero at infinity. We regain asymptotic flatness at the cost of losing the vacuum. This then leads us to the requirement that $u_0 \leq 0$ if the distorting matter is to obey the strong energy condition. We will adopt the second viewpoint. The effect of the distorting matter will be given by U and V and the Weyl metric will represent only a neighbourhood of the horizon.

Using $\psi = \psi_S + U$ and $\gamma = \gamma_S + V$, we can write the distorted Schwarzschild metric (in the usual Schwarzschild coordinates) as

$$ds^2 = -e^{2U}\left(1 - \frac{2m}{r}\right)dt^2 + e^{-2U+2V}\left[\frac{dr^2}{1-\frac{2m}{r}} + r^2 d\theta^2\right] + e^{-2U} r^2 \sin^2\theta \, d\phi^2, \quad (1.12)$$

where U and V are now functions of (r, θ). Since U and V are regular and must obey the condition in Equation 1.11, then the horizon remains at $r = 2m$. By regaining a notion of asymptotic flatness, are we then to return to defining black holes in terms of an event horizon? Not at all, since the distortions break the field equations between that neighbourhood of the horizon described by the Weyl solution and the asymptotically flat extension. The null geodesics may become discontinuous. It is possible that the event horizon still exists in these distorted spacetimes, but we have not found any verification of this hypothesis.

This uncertainty in the existence of an event horizon leads us to ask: Are there then no black holes in distorted spacetimes (and thus in more realistic situations)? Rather than throw them out, we must make use of an alternate definition of black holes; a local definition in terms of marginally trapped surfaces such as FOTHs. In the following chapter, we will examine some general properties of the distorted Schwarzschild spacetime, calculate the null normals that describe our surfaces in preparation for marginally tapped surfaces and determine appropriate distorting potentials.

CHAPTER 2

Methodology

In order to investigate the distorted Schwarzschild spacetime locally, we have three tasks ahead of us: (*a*) determine a good coordinate system; (*b*) calculate an appropriate pair of null normals; and (*c*) find appropriate solutions U and V. Once these have been completed, we can assess the existence of trapped surfaces, and thus black holes.

2.1. The Distorted Metric & A Good Coordinate System

If we recall our distorted Schwarzschild metric, Equation 1.12,

$$ds^2 = -\mathrm{e}^{2U}\left(1-\frac{2m}{r}\right)dt^2 + \mathrm{e}^{-2U+2V}\left[\frac{dr^2}{1-\frac{2m}{r}} + r^2 d\theta^2\right] + \mathrm{e}^{-2U} r^2 \sin^2\theta \, d\phi^2,$$

we notice that it is singular at the classical event horizon, $r = 2m$. We can transform to a non-singular metric with an advanced time coordinate, v, much like the Eddington-Finkelstein transformation. We let

$$t \to v - f(r,\theta) \tag{2.1}$$

where

$$f(r,\theta) = \int_{r_0}^{r} \frac{\mathrm{e}^{-2U(r',\theta)+V(r',\theta)}}{1-\frac{2m}{r'}}\, dr'$$

with r_0 an arbitrary point outside the black hole. Performing the transformation from Equation 2.1, the metric, Equation 1.12, takes the form

$$\begin{aligned} ds^2 = &-\mathrm{e}^{2U}\left(1-\frac{2m}{r}\right)dv^2 + 2\,\mathrm{e}^{V}\,dv\,dr + 2\,\mathrm{e}^{2U}\left(1-\frac{2m}{r}\right)\frac{\partial f}{\partial\theta}\,dv\,d\theta \\ &- 2\,\mathrm{e}^{V}\frac{\partial f}{\partial\theta}\,dr\,d\theta + \left[\mathrm{e}^{-2U+2V}r^2 - \mathrm{e}^{2U}\left(1-\frac{2m}{r}\right)\left(\frac{\partial f}{\partial\theta}\right)^2\right]d\theta^2 \\ &+ \mathrm{e}^{-2U}r^2\sin^2\theta\,d\phi^2, \end{aligned} \tag{2.2}$$

which is non-singular at $r = 2m$. Furthermore, when no distortions are present this reduces to the Schwarzschild metric in the usual Eddington-Finkelstein coordinates,

$$ds^2 = -\left(1-\frac{2m}{r}\right)dv^2 + 2dv\,dr + r^2d\theta^2 + r^2\sin^2\theta\,d\phi^2.$$

We can explore some general properties of the distorted Schwarzschild spacetime. Let $v = \text{const.}$ and $r = 2m$ in Equation 2.2. Then the induced metric becomes

$$ds^2 = 4\mathrm{e}^{-2U(2m,\theta)}m^2\left(\mathrm{e}^{2V(2m,\theta)}d\theta^2 + \sin^2\theta\,d\phi^2\right). \tag{2.3}$$

The first quantity we would like to know is the surface area, $\mathcal{A}$.

$$\begin{aligned} \mathcal{A} &= \int\sqrt{g_{\theta\theta}\,g_{\phi\phi}\big|_{r=2m}}\,d\theta\,d\phi \\ &= \int_0^{2\pi}\int_0^{\pi}\sqrt{16\mathrm{e}^{-4u_0}m^4\sin^2\theta}\,d\theta\,d\phi \\ &= 16\pi\,m^2\mathrm{e}^{-2u_0} \end{aligned}$$

since u_0 is a constant with respect to θ. The surface area thus depends on the value of U at the poles. When no distortion is present, $\mathcal{A} = 16\pi m^2$ as expected for the Schwarzschild event horizon.

The Gaussian curvature, $\mathscr{K}$, can be found using [**32**]

$$\mathscr{K} = -\frac{1}{\sqrt{g_{\theta\theta}g_{\phi\phi}}}\left[\frac{\partial}{\partial\theta}\left(\frac{1}{\sqrt{g_{\theta\theta}}}\frac{\partial\sqrt{g_{\phi\phi}}}{\partial\theta}\right)+\frac{\partial}{\partial\phi}\left(\frac{1}{\sqrt{g_{\phi\phi}}}\frac{\partial\sqrt{g_{\theta\theta}}}{\partial\phi}\right)\right].$$

The value we obtain for the Gaussian curvature of the horizon is then

$$\mathscr{K} = \frac{1}{4m^2}\mathrm{e}^{2U-2V}\left[1+\frac{\partial U}{\partial\theta}\left(\cot\theta-\frac{\partial V}{\partial\theta}\right)+\cot\theta\frac{\partial V}{\partial\theta}+\frac{\partial^2 U}{\partial\theta^2}\right]$$

where U, V and their derivatives are evaluated on the horizon. Since U, V and their derivatives are regular at the horizon, then $\mathscr{K}$ also remains regular at the horizon. When no distortion is present, $\mathscr{K} = \frac{1}{4m^2}$ as expected for the Schwarzschild event horizon.

The Kretschmann scalar provides a demonstration that the distorted spacetime is regular at the horizon. It is given by

$$\begin{aligned}
\mathcal{K}\big|_{r=2m} &= R_{abcd}R^{abcd}\big|_{r=2m} \\
&= \frac{1}{4m^4}\mathrm{e}^{8u_0-4U}\Bigg[3-16\cot\theta\left(\frac{\partial U}{\partial\theta}\right)^3+7\left(\frac{\partial U}{\partial\theta}\right)^4+3\left(\frac{\partial^2 U}{\partial\theta^2}\right)^2 \\
&\quad+2\cot\theta\frac{\partial U}{\partial\theta}\left(4+3\frac{\partial^2 U}{\partial\theta^2}-2m\frac{\partial U}{\partial r}\right)+4\frac{\partial^2 U}{\partial\theta^2}\left(1-m\frac{\partial U}{\partial r}+m\frac{\partial V}{\partial r}\right) \\
&\quad+\left(\frac{\partial U}{\partial\theta}\right)^2\left(11\csc^2\theta-19-4\frac{\partial^2 U}{\partial\theta^2}+12m\frac{\partial U}{\partial r}-2m\frac{\partial V}{\partial r}\right) \\
&\quad+m\left(20m\left(\frac{\partial U}{\partial r}\right)^2-12\frac{\partial U}{\partial r}\left(1+m\frac{\partial V}{\partial r}\right)+\frac{\partial V}{\partial r}\left(4+3m\frac{\partial V}{\partial r}\right)\right)\Bigg]
\end{aligned}$$

where we have used Equation 1.11 to simplify the resulting expression. Again, since U, V and their derivatives are regular at the horizon, $\mathcal{K}$ remains regular at the horizon.

showing that no new singularities appear in distorted Schwarzschild spacetime. When no distortion is present, $\mathcal{K} = \frac{3}{4m^4}$ as expected for the Schwarzschild event horizon.

Finally, we are interested in the surface gravity of the horizon. The surface gravity, κ_G, is defined by a Killing vector [**29**],

$$\xi^a_{;b}\xi^b = \kappa_G \xi^a.$$

This definition is not unique, since ξ could be rescaled by a constant which will will also scale κ_G. Thus, the surface gravity we calculate will only be defined up to constant rescaling. The Killing vector we will use is $\xi^a = \left(\frac{\partial}{\partial v}\right)^a$ which satisfies Killing's equation, $\xi_{a;b} + \xi_{b;a} = 0$. Then, the surface gravity is

$$\kappa_G^2 = -\frac{1}{2}\left(\xi_{a;b}\right)\left(\xi^{a;b}\right) = \frac{1}{16m^2}\mathrm{e}^{4u_0} \qquad \Longrightarrow \qquad \kappa_G = \frac{1}{4m}\mathrm{e}^{2u_0}. \tag{2.4}$$

When no distortion is present, $\kappa_G = \frac{1}{4m}$ as expected for the Schwarzschild event horizon. Furthermore, notice that Smarr's formula holds for the distorted Schwarzschild spacetime [**31**],

$$\begin{aligned}\frac{\kappa_G \mathcal{A}}{4\pi} &= \frac{1}{4\pi}\left(\frac{1}{4m}\mathrm{e}^{2u_0}\right)\left(16\pi\, m^2 \mathrm{e}^{-2u_0}\right) \\ &= \frac{1}{4\pi}\left(4\pi\, m\right) \\ &= m.\end{aligned}$$

With our good coordinate system, we now turn our attention to the null normals, ℓ_a and n_a. We will use these to determine the inward and outward expansion of the distorted Schwarzschild spacetime.

2.2. Null Normals

The hypersurface defined by $r = 2m$ has two null normals: an outward null normal and an inward null normal. There are three requirements for an appropriate outward null normal: (*a*) $\ell_a \propto dr$ on the horizon (ℓ_a points outwards); (*b*) $\ell^v > 0$ on the horizon (ℓ^a points forward in time); and (*c*) $\ell_a \ell^a = 0$ everywhere (ℓ_a is null.) To accommodate these requirements, we choose our outward null normal to be

$$\ell_a = \left(-\frac{1}{2}\left[1 - \frac{2m}{r}\right],\ \frac{1}{2}\mathrm{e}^{-2U}\left\{ \mathrm{e}^{V} + \sqrt{\mathrm{e}^{2V} - \frac{1}{r^2}\mathrm{e}^{4U}\left[1 - \frac{2m}{r}\right]\left[\frac{\partial f}{\partial \theta}\right]^2} \right\},\ 0,\ 0 \right). \tag{2.5}$$

On the horizon, the normal and associated vector take the forms

$$\ell_a\Big|_{r=2} = \left(0,\ \mathrm{e}^{-2u_0},\ 0,\ 0\right)$$
$$\ell^a\Big|_{r=2} = \left[\mathrm{e}^{-2U},\ 0,\ 0,\ 0\right]$$

and it can be verified that $\ell_a \ell^a = 0$ everywhere. Thus, conditions (a), (b) and (c) are satisfied.

The inward null normal can be calculated from a combination of the outward null normal and another normal associated with the horizon. To foliate the horizon, we will consider the set of surfaces

$$\Sigma_\sigma = \left\{ (v,\ 2m,\ \theta,\ \phi) \mid v - S(\theta) = \sigma \right\} \tag{2.6}$$

where $\sigma \in \mathbb{R}$ is a label for the surfaces and $S(\theta) \in C^\infty$ characterizes the foliation. We choose a general foliation of the spacetime, since the standard foliation may not provide marginally trapped surfaces. Furthermore, notice that the properties discussed in the previous section made no mention of this foliation. We have that ℓ_a

is one normal to this surface and

$$\omega_a = \left[dv\right]_a - S'(\theta)\left[d\theta\right]_a$$

is another normal, though not necessarily null.

To ensure that we have a second null normal, we take the combination

$$n_a = \beta\left(\alpha\,\ell_a + \omega_a\right).$$

Our conditions on n_a are: (a) $n_a n^a = 0$; and (b) $\ell_a n^a = -1$. And so we find that

$$\alpha = -\frac{\omega_a\omega^a}{2\ell_a\omega^a} \qquad\qquad \beta = -\frac{1}{\ell_a\omega^a}.$$

The null normal we end up with is

$$n_a = \Bigg(-\frac{\mathrm{e}^{2U+2V}\left\{2\mathrm{e}^V\left[\mathrm{e}^V + \mathfrak{F}(r,\theta)\right] + \mathrm{e}^{4U}h(r)\left[\left(\frac{dS}{d\theta}\right)^2 - \left(\frac{\partial f}{\partial\theta}\right)^2\right]\right\}}{\mathfrak{R}(r,\theta)^2},$$
$$\frac{\mathrm{e}^{4U+2V}\left[\mathrm{e}^V + \mathfrak{F}(r,\theta)\right]\left[\frac{dS}{d\theta} - \frac{\partial f}{\partial\theta}\right]^2}{r^2\,\mathfrak{R}(r,\theta)^2},\ \frac{2\mathrm{e}^{2U+2V}\frac{dS}{d\theta}}{\mathfrak{R}(r,\theta)},\ 0\Bigg) \tag{2.7}$$

where

$$\mathfrak{R}(r,\theta) = \mathrm{e}^V\left[\mathrm{e}^V + \mathfrak{F}(r,\theta)\right] + \mathrm{e}^{4U}h(r)\,\frac{\partial f}{\partial\theta}\left[\frac{dS}{d\theta} - \frac{\partial f}{\partial\theta}\right],$$

$$\mathfrak{F}(r,\theta) = \sqrt{\mathrm{e}^{2V} - \mathrm{e}^{4U}h(r)\left(\frac{\partial f}{\partial\theta}\right)^2}$$

and

$$h(r) = \frac{1}{r^2}\left(1 - \frac{2m}{r}\right).$$

Two of our three tasks are complete; on to the distorting potentials U and V.

2.3. Distorting Potentials

Recall that U satisfies Laplace's equation, (1.7),

$$\frac{\partial^2 U}{\partial \rho^2} + \frac{1}{\rho}\frac{\partial U}{\partial \rho} + \frac{\partial^2 U}{\partial z^2} = 0.$$

We consider a multipole expansion in the Legendre polynomials. The multipole expansion of a Newtonian potential is well known. The use of multipole expansions in general relativity began with Geroch [**33**] and Hansen [**34**], with Thorne [**35**] providing a common framework focussing on gravitational waves. Let [**28**]

$$U(\rho, z) = \sum_{i=1}^{\infty} a_i \left(\rho^2 + z^2\right)^{\frac{i}{2}} P_i\left(\frac{z}{\sqrt{\rho^2 + z^2}}\right).$$

We can transform this solution to Schwarzschild coordinates,

$$U(r, \theta) = \sum_{i=1}^{\infty} \alpha_i m^{-i} \left[r^2\left(1 - \frac{2m}{r}\right) + m^2 \cos^2\theta\right]^{\frac{i}{2}} P_i\left(\frac{(r-m)\cos\theta}{\sqrt{r^2\left(1 - \frac{2m}{r}\right) + m^2\cos^2\theta}}\right). \tag{2.8}$$

On the horizon, $r = 2m$, so

$$U = \sum_{i=1}^{\infty} \alpha_i \cos^i\theta P_i(1) = \sum_{i=1}^{\infty} \alpha_i \cos^i\theta.$$

Notice that at the north pole $\Big[(r, \theta) = (2m, 0)$ or $(\rho, z) = (0, 1)\Big]$ we have

$$U = \sum_{i=1}^{\infty} \alpha_i,$$

but at the south pole $\Big[(r, \theta) = (2m, \pi)$ or $(\rho, z) = (0, -1)\Big]$ we have

$$U = \sum_{i=1}^{\infty} (-1)^i \alpha_i.$$

To ensure elementary flatness, i.e. the condition that $U(2m,0) = U(2m,\pi) = u_0$, we must have

$$\sum_{k=1}^{\infty} \alpha_{2k+1} = 0. \tag{2.9}$$

This leads to

$$u_0 = \sum_{k=1}^{\infty} \alpha_{2k}. \tag{2.10}$$

So, if the distorting matter obeys the strong energy condition, then the sum of the even multipoles will be non-positive and that of the odd multipoles will be zero.

From the solution for U we can calculate V since, from Equation 1.8, we get

$$\frac{\partial V}{\partial \rho} = \rho \left[\left(\frac{\partial V}{\partial \rho} \right)^2 - \left(\frac{\partial V}{\partial z} \right)^2 + 2 \left(\frac{\partial \psi_S}{\partial \rho} \frac{\partial U}{\partial \rho} + \frac{\partial \psi_S}{\partial z} \frac{\partial U}{\partial z} \right) \right]$$

and

$$\frac{\partial V}{\partial z} = 2\rho \left[\frac{\partial U}{\partial \rho} \frac{\partial U}{\partial z} + \frac{\partial \psi_S}{\partial \rho} \frac{\partial U}{\partial z} + \frac{\partial \psi_S}{\partial z} \frac{\partial U}{\partial \rho} \right].$$

Using these, we get (in Schwarzschild coordinates) [**28**]

$$\begin{aligned} V(r,\theta) = \sum_{i=1}^{\infty} \alpha_i \sum_{j=0}^{i-1} \Bigg\{ & m^{-(j+1)} \Big[(-1)^{i-j+1} (r - m + m\cos\theta) \\ & - r + m + m\cos\theta \Big] \left[r^2 \left(1 - \frac{2m}{r} \right) + m^2 \cos^2\theta \right]^{\frac{j}{2}} P_j \Bigg\} \\ & + \sum_{i=1}^{\infty} \alpha_i^2 \frac{i}{2m^{2i}} \left[r^2 \left(1 - \frac{2m}{r} \right) + m^2 \cos^2\theta \right]^i \left[P_i^2 - P_{i-1}^2 \right] \end{aligned} \tag{2.11}$$

where $P_k \equiv P_k\Big([r-m]\cos\theta \left[r^2 \left(1 - \frac{2m}{r} \right) + m^2 \cos^2\theta \right]^{-\frac{1}{2}} \Big)$ as in U. At the north pole,

$$V = -\sum_{i=1}^{\infty} \left[(-1)^i - 1 \right] \alpha_i = 0$$

since $2\sum_{i=1}^{\infty}\alpha_{2i+1} = 0$ and $(-1)^{2i} - 1 = 0$. Similarly, at the south pole,

$$V = \sum_{i=1}^{\infty}\left[(-1)^i - 1\right]\alpha_i = 0.$$

And so, the conditions from Equation 2.9 and Equation 2.10 give local flatness which fixes the location of the horizon at $r = 2m$. Not only that, but we also achieve an equilibrium situation since, if there were no local flatness, the black hole would experience a tidal force [**19**]. Equipped with our metric in a good coordinate system, appropriate null normals and distorting potentials, we are at a point where we can calculate the expansion scalars. The expansion scalars and the existence of marginally trapped surfaces will be the subject of the next chapter.

CHAPTER 3

Results and Discussion

We have seen that the event horizon does not provide an adequate local description of a black hole. To remedy this situation, we introduced the future outer trapping horizon (FOTH) which relies on the local concepts of the expansion scalar and Lie derivative. In this chapter, we will seek to determine whether the distorted Schwarzschild spacetime detailed in the previous chapter can be described by FOTHs.

First, we shall calculate the expansion scalars, Θ, for which the sign of the inward expansion, $\Theta_{(n)}$, cannot be determined in the general case, but rather only for specified foliations and multipole moments. We then choose a foliation to work with, surprisingly the chosen foliation turns out to be surfaces of constant Schwarzschild time. Then we find that the actual value of the Lie derivative does not matter, so long as other properties of the spacetime hold. Finally, we investigate specific multipole moments and briefly examine alternate foliations.

3.1. Expansion Scalars

With the null normals, ℓ_a and n_a, derived in the previous chapter we are now in a position to calculate the expansion scalars. Recall the that the induced metric is given by

$$q_{ab} = g_{ab} + \ell_a n_b + n_a \ell_b$$

and the expansion scalar of a congruence of null geodesics with tangent k^a is given by

$$\Theta_{(k)} = q^{ab} k_{a;b}.$$

Then the expansion of the outward null normal at the horizon is given by

$$\Theta_{(\ell)} = 0,$$

as expected from the construction of ℓ_a in Equation 2.5, and the inward expansion is given by

$$\Theta_{(n)} = \frac{1}{16m^3} e^{2U-3V} \left\{ e^{4U} \left(\frac{dS}{d\theta} - \frac{\partial f}{\partial \theta} \right)^2 + 16 e^{2V} m^2 \left(2m \frac{\partial U}{\partial r} - m \frac{\partial V}{\partial r} - 1 \right) \right.$$
$$\left. + 4 e^{2U+V} m \left[\frac{d^2 S}{d\theta^2} - \frac{\partial^2 f}{\partial \theta^2} + \cot\theta \left(\frac{dS}{d\theta} - \frac{\partial f}{\partial \theta} \right) \right] \right\}, \tag{3.1}$$

where f, U, V and their derivatives are evaluated on the horizon. We see that the inward expansion depends not only on the distorting potentials but also the foliation, as expected from the definition of n_a in Equation 2.7.

3.2. Standard Foliation

If we were to use the standard foliation, $S(\theta) = 0$, then the inward expansion scalar would be

$$\Theta_{(n)} = \frac{1}{16m^3} e^{6u_0} \left(\frac{\partial f}{\partial \theta} \right)^2 - \frac{1}{4m^2} e^{4u_0} \left(\cot\theta \frac{\partial f}{\partial \theta} + \frac{\partial^2 f}{\partial \theta^2} \right)$$
$$+ \frac{1}{m} e^{2u_0} \left(2m \frac{\partial U}{\partial r} - m \frac{\partial V}{\partial r} - 1 \right), \tag{3.2}$$

where U, V, f and their derivatives are evaluated at the horizon. Notice that when no distortions are present $\left(\text{i.e. } u_0 = U = V = \frac{\partial f}{\partial \theta} = 0\right)$ we get $\Theta_{(n)} = -\frac{1}{m}$ as expected.

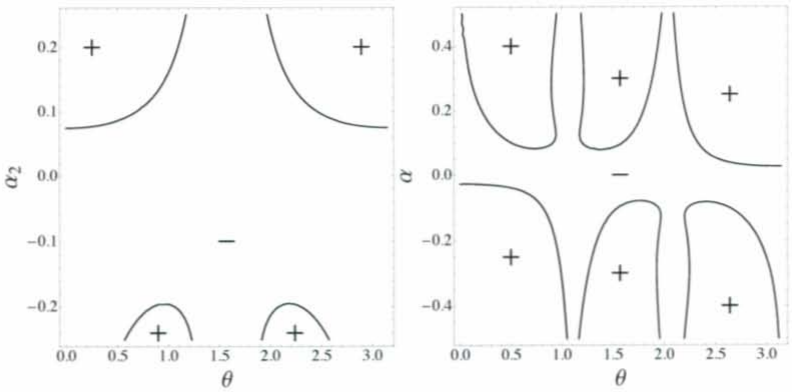

(A) Expansion for quadrupolar distortion with the standard foliation.

(B) Expansion for dip-octupolar distortion with the standard foliation.

FIGURE 3.1. Expansion scalars for the standard foliation.

When we plot the positive and negative regions of Equation 3.2 for quadrupole, $i = 2$, (Figure 3.1a) and dipole-octupole, $i = 1$ & 3, (Figure 3.1b) distortions, we find very limited ranges of multipole moments where marginally trapped surfaces could exist. The standard foliation, then, is perhaps not the best choice.

3.3. Improved Foliation

Ideally, from Equation 3.1, we would like to solve $\Theta_{(n)} < 0$ for $S(\theta)$ so that we have a general foliation of the spacetime. Unfortunately, deriving a general solution appears to be an insurmountable task. If we let $\Theta_{(n)} < 0$, say $\Theta_{(n)} = -\frac{e^{2u_0}}{m}$, then we notice that Equation 3.1 can be put in the form of a Riccati equation, [**36**],

$$\frac{dy}{d\theta} = q_0(\theta) + q_1(\theta)\, y(\theta) + q_2(\theta)\, y(\theta)^2$$

where $y = \frac{dS}{d\theta}$. This equation does not have a general solution, except for relatively simple q_i's, which is not the case for Equation 3.1. Instead, we will attempt to construct a solution. Examining Equation 3.1, we notice that a choice of

$$\frac{dS}{d\theta} = \frac{\partial f}{\partial \theta} \qquad \Longrightarrow \qquad S(\theta) = f(2m, \theta) = \int_{r_0}^{2m} \frac{e^{-2U(r',\theta)+V(r',\theta)}}{1 - \frac{2m}{r'}} dr', \tag{3.3}$$

where r_0 is a point outside of the Schwarzschild radius, simplifies $\Theta_{(n)}$ substantially. Substituting Equation 3.3, we get

$$\Theta_{(n)} = \frac{1}{m} e^{2u_0} \left[2m \frac{\partial U}{\partial r} - m \frac{\partial V}{\partial r} - 1 \right]. \tag{3.4}$$

It is thought that this should improve the range of multipole moment magnitudes so that FOTHs can be present for all multipole moments.

Recall the surfaces that we chose to foliate the distorted spacetime in Equation 2.6,

$$\Sigma_\sigma = \Big\{ (v,\ 2m,\ \theta,\ \phi) \mid v - S(\theta) = \sigma \Big\}.$$

Notice that the description of the foliating surfaces also simplifies since, from Equation 2.1

$$\begin{aligned} \Big[v - S(\theta) \Big] \Big|_{r=2m} &= t + f(2m, \theta) - S(\theta) \\ &= t + f(2m, \theta) - f(2m, \theta) \\ &= t. \end{aligned}$$

Our foliations are simply slices of constant Schwarzschild time. That is, the set of points

$$\Sigma_t = \left\{ (t,\ 2m,\ \theta,\ \phi) \;\middle|\; t \in \mathbb{R},\ 0 \leq \theta < \pi,\ 0 \leq \phi < 2\pi \right\}.$$

If we now substitute the solutions for U, Equation 2.8, and V, Equation 2.11, into $\Theta_{(n)}$, Equation 3.4, we get

$$\Theta_{(n)} = \frac{1}{m} e^{\sum_{i=1}^{\infty}\left(1+(-1)^i\right)\alpha_i}\left[\sum_{i=1}^{\infty}\left(2\,i\,\cos^i\theta\,\alpha_i + i^2\cos^{2(i-1)}\theta\,\sin^2\theta\,\alpha_i^2\right) - 1\right]. \qquad (3.5)$$

To determine the existence of marginally trapped surfaces, we will examine individual multipole moments (i.e. finitely many terms in Equation 3.5.) However, from the elementary flatness condition on the $\rho = 0$ axis,

$$u_0 = \sum_{i=1}^{\infty}\alpha_{2i} \qquad \text{and} \qquad 0 = \sum_{i=1}^{\infty}\alpha_{2i+1},$$

means that we cannot have individual odd multipole moments, and that individual even multipole moments must be negative if the strong energy condition is to be satisfied. Below, we will examine a few cases in greater detail: a purely quadrupole ($i = 2$) distortion; a purely hexadecapole ($i = 4$) distortion; a dipole-octupole ($i = 1$ & 3) distortion; and finally a dipole-quadrupole-octupole ($i = 1$, 2 & 3) distortion. Before we can perform these calculations, however, we must tackle the second condition of our marginally trapped surfaces to foliate a FOTH, the value of the Lie derivative, $\mathcal{L}_n\Theta_{(\ell)} < 0$.

3.4. Lie Derivative

Recall the requirements for $\mathcal{H}$ to be a future outer trapping horizon:

i. $\Theta_{(\ell)} = 0$ and $\Theta_{(n)} < 0$; and

ii. $\mathcal{L}_n\Theta_{(\ell)} < 0$.

It would be convenient if there were another way of determining the second condition since, if we naïvely calculate the Lie derivative of $\Theta_{(\ell)}$ along n^a, we get

$$\mathcal{L}_n\Theta_{(\ell)} = \Theta_{(\ell),a}n^a = \frac{\mathrm{e}^{6U-4V}}{64m^4}\left(\frac{\partial f}{\partial\theta}\right)^2 + \frac{\mathrm{e}^{4U-3V}}{16m^3}\left[\frac{\partial f}{\partial\theta}\left(\cot\theta + 2\frac{\partial U}{\partial\theta} - \frac{\partial V}{\partial\theta}\right) + \frac{\partial^2 f}{\partial\theta^2}\right] + \frac{\mathrm{e}^{2U-2V}}{4m^2}\left[2m\frac{\partial U}{\partial r} - m\frac{\partial V}{\partial r} - 1\right] \tag{3.6}$$

where again f, U, V and their derivatives are evaluated on the horizon. Not a very pleasant result. Consider again Figure 1.4. When we travel along n^a, we may not end up on a proper, distorted slice of spacetime even though we have evolved along the tangent to the congruence. We may, instead, be calculating on a surface that crosses between different slices. Rather than perform this cumbersome—and possibly wrong—calculation, we will instead consider how our marginally trapped surfaces change under infinitesimal deformations, $\delta_n\Theta_{(\ell)}$, so that the surfaces become fully trapped, $\Theta_{(n)} < 0$ and $\Theta_{(\ell)} < 0$. The deformations will be described by [**37**]

$$\delta_{(n)}\Theta_{(\ell)} = -\mathscr{K} + \tilde{\omega}^a\tilde{\omega}_a - d_a\tilde{\omega}^a + 8\pi T_{ab}\ell^a n^b \tag{3.7}$$

where $\mathscr{K}$ is the Gaussian curvature on the horizon, $\tilde{\omega}_a = -q^b{}_a n_c \ell^c{}_{;b}$ is the connection form, d_a is the covariant derivative compatible with the induced metric, q_{ab}, and T_{ab} is the stress-energy tensor. The evolution of $\Theta_{(n)}$ is given by the following, analogous to Raychaudhuri's equation [**37**],

$$\mathcal{L}_\ell\Theta_{(n)} + \kappa_G\,\Theta_{(n)} = -\mathscr{K} + \tilde{\omega}^a\tilde{\omega}_a + d_a\tilde{\omega}^a + 8\pi T_{ab}\ell^a n^b. \tag{3.8}$$

If we now subtract Equation 3.8 from Equation 3.7, we find

$$\delta_{(n)}\Theta_{(\ell)} - \mathcal{L}_\ell\Theta_{(n)} - \kappa_G\,\Theta_{(n)} = -2\,d^a\tilde{\omega}_a.$$

We know that $\mathcal{L}_\ell \Theta_{(n)} = 0$ and it can be shown that there always exists a scaling (say, ℓ_0^a) such that $d^a \tilde{\omega}_a = 0$. Consider a pair of null vectors $(\ell_0^a,\ n_0^a)$ such that

$$\ell^a = \frac{1}{\mathfrak{f}}\,\ell_0^a \qquad \text{and} \qquad n^a = \mathfrak{f}\, n_0^a,$$

as well as

$$\overline{\ell}^a = \mathfrak{f}\,\ell_0^a \qquad \text{and} \qquad \overline{n}^a = \frac{1}{\mathfrak{f}}\, n_0^a.$$

Then

$$\delta_{(\overline{n})}\Theta_{(\overline{\ell})} = \kappa_G \Theta_{(n)}.$$

What this means is that, since $\Theta_{(n)} < 0$ for trapped surfaces (either fully or marginally), we need only to check that there exists a scaling such that $\kappa_G > 0$ for the deformation to be negative and thus satisfy the second condition for our surfaces to describe a FOTH. Recall the surface gravity we calculated in the previous chapter, Equation 2.4,

$$\kappa_G = \frac{1}{4m} e^{2u_0}.$$

Since $m > 0$ and $u_0 \in \mathbb{R}$, κ_G will always be positive; we already have the desired scaling. Therefore, so long as the first condition is satisfied, we will always be able to locate a FOTH. With both conditions determined, we shall now investigate specific cases of the distorted Schwarzschild spacetime.

3.5. Distorted Schwarzschild Spacetime

For any further numerical calculations, we will set $m = 1$. We can fix this value because the expansion scalar, Equation 3.5, depends only on the inverse of m. Since m is a positive constant, its exact value will not affect the sign of $\Theta_{(n)}$. The numerical investigations into the values of α_i will be performed using Mathematica.

3.5.1. External Quadrupole Field. In this section, we will examine a Schwarzschild spacetime in a background quadrupole ($i = 2$) field. In that case, the expansion will be given by

$$\Theta_{(n)} = -\mathrm{e}^{2\alpha_2}\left[1 - 4\cos^2\theta\,\alpha_2 - \sin^2 2\theta\,\alpha_2^2\right]. \tag{3.9}$$

Recall that elementary flatness requires that $u_0 = \sum_{k=1}^{\infty}\alpha_{2k}$, so for a purely quadrupolar distortion,

$$u_0 = \sum_{k=1}^{\infty}\alpha_{2k}\delta_{k1} = \alpha_2$$

where δ_{lm} is the usual Kronecker delta. For matter to satisfy the strong energy condition, $u_0 \leq 0$, so

$$\alpha_2 \leq 0.$$

The most convenient way to begin our investigation is by plotting $\Theta_{(n)}$, as shown in Figure 3.2

As we can see, there is a certain range for which $\Theta_{(n)} < 0$. The maximum positive value, α_2^+, is obtained when $\theta = 0$ or π. Then Equation 3.9 becomes

$$\Theta_{(n)}\Big|_{\theta=0} = -\mathrm{e}^{2\alpha_2}\,(1 - 4\alpha_2)$$

and so we find that the maximum positive value of α_2 is given by

$$\alpha_2^+ = \frac{1}{4}.$$

Similarly, the maximum negative value is given by

$$\alpha_2^- = -2.$$

Thus, the range of α_2 values for which $\Theta_{(n)} < 0$ is $-2 \leq \alpha_2 \leq \frac{1}{4}$. For the distorting matter to satisfy the strong energy condition, the range is reduced to non-positive

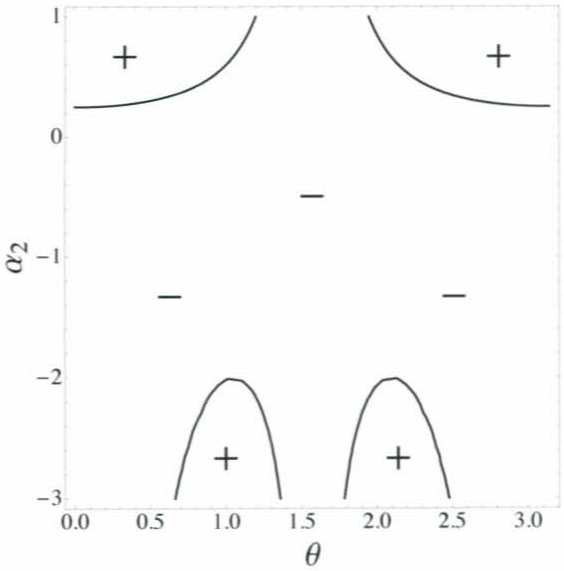

FIGURE 3.2. Graph showing the positive and negative regions of $\Theta_{(n)}$ in a quadrupole distortion.

values. Therefore we will say that, with our chosen foliation, a FOTH will be present in quadrupolarly distorted Schwarzschild spacetime when the magnitude of the distortions, α_2, falls within the range $-2 \leq \alpha_2 \leq 0$.

We can also investigate the geometry of the horizon under a quadrupolar distortion using an embedding diagram. Since the horizon is a 2-surface, it may be possible to embed it in a flat three-dimensional space. The manner in which we accomplish these diagrams is as follows. Recall the induced metric (with $m = 1$), Equation 2.3,

$$ds^2 = 4\mathrm{e}^{-2U(2,\theta)}\left(\mathrm{e}^{2V(2,\theta)}d\theta^2 + \sin^2\theta d\phi^2\right), \tag{3.10}$$

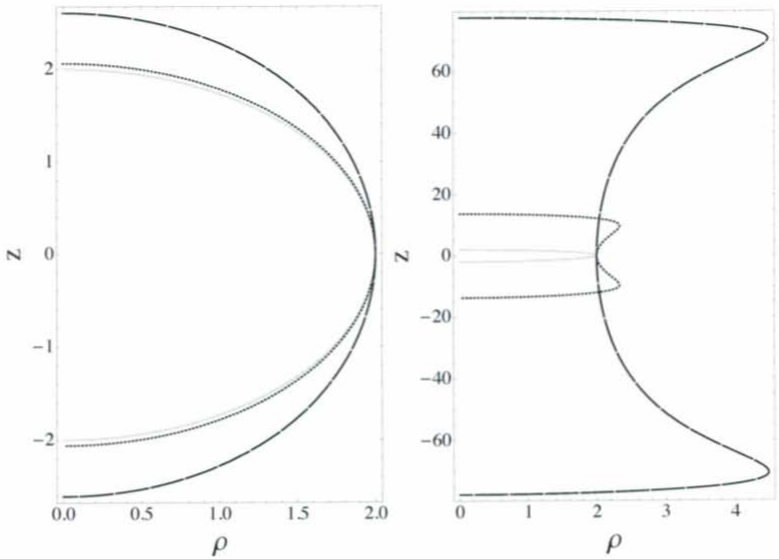

(A) Embedding diagram for small values of α_2 (-0.01 and -0.1) and an undistorted horizon.

(B) Embedding diagram for large values of α_2 (-1 and -2) and an undistorted horizon.

FIGURE 3.3. Embedding diagrams for a quadrupolarly distorted horizon.

and consider a fictitious Euclidean 3-space described by the metric

$$d\Sigma^2 = ds^2 + s^2 d\phi^2 + dz^2.$$

Now, we can perform an embedding by letting $s = s(\theta)$ and $z = z(\theta)$. Substituting these into the flat metric, we get

$$d\Sigma^2 = \left[z'(\theta)^2 + s'(\theta)^2\right] d\theta^2 + s(\theta)^2 d\phi^2. \tag{3.11}$$

Then we compare coefficients of Equation 3.10 with those of Equation 3.11 to find

$$s(\theta)^2 = 4\mathrm{e}^{-2U}\sin^2\theta$$

and

$$z'(\theta)^2 + s'(\theta)^2 = 4\mathrm{e}^{-2U+2V}.$$

Solving for $s(\theta)$ and $z(\theta)$, we find

$$s(\theta) = 2\mathrm{e}^{-U(2,\theta)}\sin\theta \tag{3.12}$$

and

$$z(\theta) = -2\int_0^\theta \mathrm{e}^{-U(2,\theta')}\sqrt{\mathrm{e}^{2V(2,\theta')} - \left(\cos\theta' - \sin\theta'\frac{\partial U}{\partial\theta'}\right)^2}\,d\theta' \tag{3.13}$$

where $z(\theta)$ can easily be numerically integrated using the known functions U and V. The presence of a square root in the integrand above may be cause for concern: might there be some region where embeddings are not possible? For the quadrupole, it turns out there is a range, which coincides with the strong energy condition. So long as $\alpha_2 \leq 0$, we can perform an embedding.

In Figure 3.3, we see the embedding diagrams for different values of α_2. In both figures, the grey line represents an undistorted horizon, $\alpha_2 = 0$. Figure 3.3a shows relatively small values of α_2; the dotted line represents $\alpha_2 = -\frac{1}{100}$ and the dashed line represents $\alpha_2 = -\frac{1}{10}$. For such distortions, the horizon retains a spheroidal geometry—the horizon is pulled away from the poles, but the equator remains fixed. For larger distortions, as in Figure 3.3b, the geometry of the horizon is no longer spheroidal. In this plot, the dotted line is for $\alpha_2 = -1$ and the dashed line for $\alpha_2 = -2$. Again, the equator remains fixed, while the poles are stretched. Not only

are the poles stretched but, at $\theta = \frac{\pi}{4}$ for $\alpha_2 = -1$ and $\theta = \frac{\pi}{6}$ for $\alpha_2 = -2$, the horizon is stretched quite drastically.

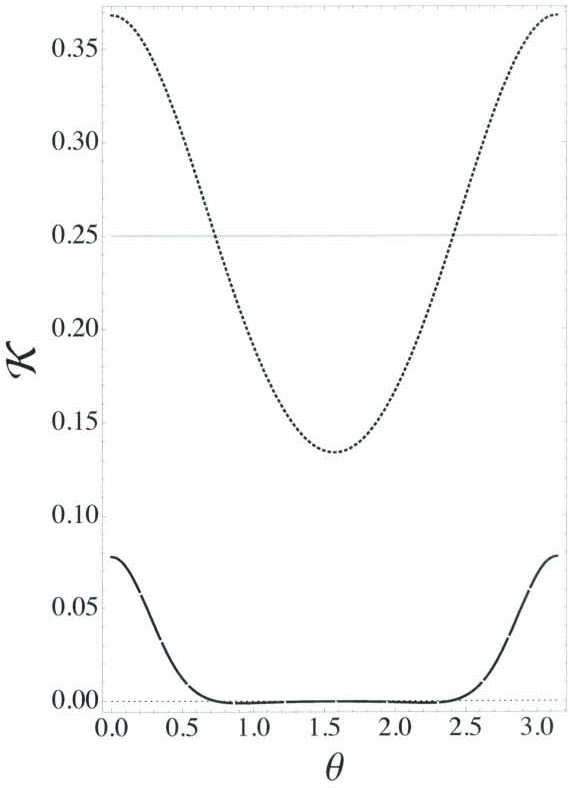

FIGURE 3.4. Gaussian curvature of the horizon for a quadrupole distortion for $\alpha_2 = 0, -\frac{1}{10}$ and -2.

This is not so surprising if we were to look at the Gaussian curvature. Recall, from section 2.1, the Gaussian curvature is given by

$$\mathscr{K} = \frac{1}{4m^2} e^{2U-2V} \left[1 + \frac{\partial U}{\partial \theta} \left(\cot\theta - \frac{\partial V}{\partial \theta} \right) + \cot\theta \frac{\partial V}{\partial \theta} + \frac{\partial^2 U}{\partial \theta^2} \right].$$

For a quadrupole distortion we get (with $m = 1$),

$$\mathscr{K} = \frac{1}{4} e^{-\alpha_2(\cos 2\theta - 3)} \left[1 - (3 + 5\cos 2\theta)\,\alpha_2 + (\cos 4\theta - 1)\,\alpha_2^2 \right].$$

If we plot this for some of the values of α_2 from Figure 3.3, we see from Figure 3.4 that the Gaussian curvature changes sign for sufficiently large values of α_2. The grey line is positive and constant as expected for undistorted Schwarzschild spacetime; the surface is a sphere. The dotted line represents $\alpha_2 = -\frac{1}{10}$ and is always positive, though not constant. The dashed line represents $\alpha_2 = -2$ and notice that it goes negative (the dotted grey line is zero curvature); the geometry deviates from spheroidal.

3.5.2. External Hexadecapole Field. We now examine the hexadecapole ($i = 4$) distortion. Similarly to the quadrupole distortion, we have $u_0 = \sum_{k=1}^{\infty} \alpha_{2k}\delta_{k2} = \alpha_4$ to satisfy elementary flatness and $\alpha_4 \leq 0$ if the distorting matter satisfies the strong energy condition. From Figure 3.5, we again see that there is a range of values for α_4. The maximum positive value will be

$$\alpha_4^+ = \frac{1}{8}$$

and the maximum negative value will be

$$\alpha_4^- \approx -2.37.$$

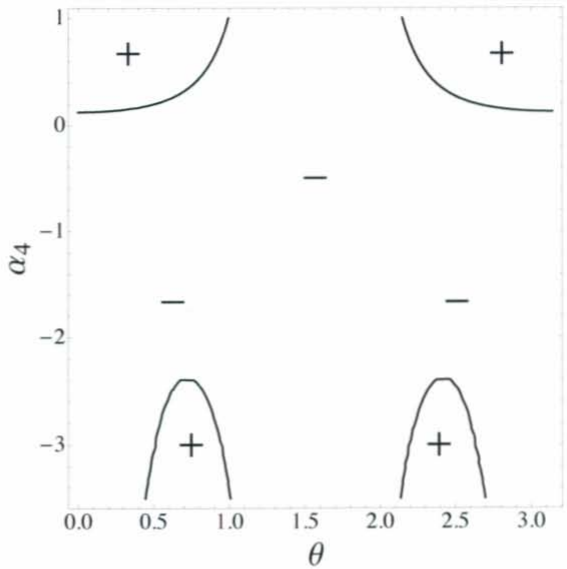

FIGURE 3.5. Graph showing the positive and negative regions of $\Theta_{(n)}$ in a hexadecapole distortion.

Therefore, the range of possible values for a hexadecapole field is $-2.37 < \alpha_4 \leq \frac{1}{8}$. For a FOTH to be present in our chosen foliation (and for the distorting matter to satisfy the strong energy condition), the magnitude of the distortion must fall in the range $-2.37 < \alpha_4 \leq 0$.

We can also examine the embedding diagrams of the horizon in an external hexadecapole field, shown in Figure 3.6. Like the quadrupole, small distortions retain the overall spheroidal shape but stretch at the poles. Strong distortions will stretch the horizon into odd shapes, as seen in Figure 3.6b. Four values of α_4 are shown: the grey line shows an undistorted horizon; the dotted line shows $\alpha_4 = -1$; the dashed line shows $\alpha_4 = -1.2$; and the dot-dashed line shows $\alpha_4 = -2.3$.

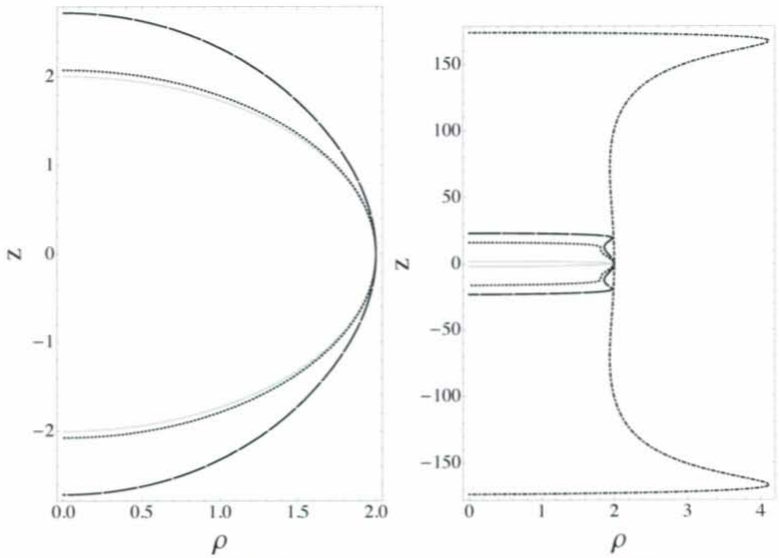

(A) Embedding diagram for small values of α_4 (-0.01 and -0.1) and an undistorted horizon.

(B) Embedding diagram for large values of α_4 (-1, -1.2 and -2.3) and an undistorted horizon.

FIGURE 3.6. Embedding diagrams for a hexadecapolarly distorted horizon.

As in the quadrupole case, if we plot the Gaussian curvature for some of the values of α_4 from Figure 3.6, we see from Figure 3.7 that there are sign changes for sufficiently large values of α_4. The grey line is positive and constant as expected for undistorted Schwarzschild spacetime; the surface is a sphere. The dotted line represents $\alpha_4 = -\frac{1}{10}$ and is always positive, though not constant. The dashed line represents $\alpha_4 = -2.37$ and notice that it goes negative (the dotted grey line is zero curvature); the geometry deviates from spheroidal.

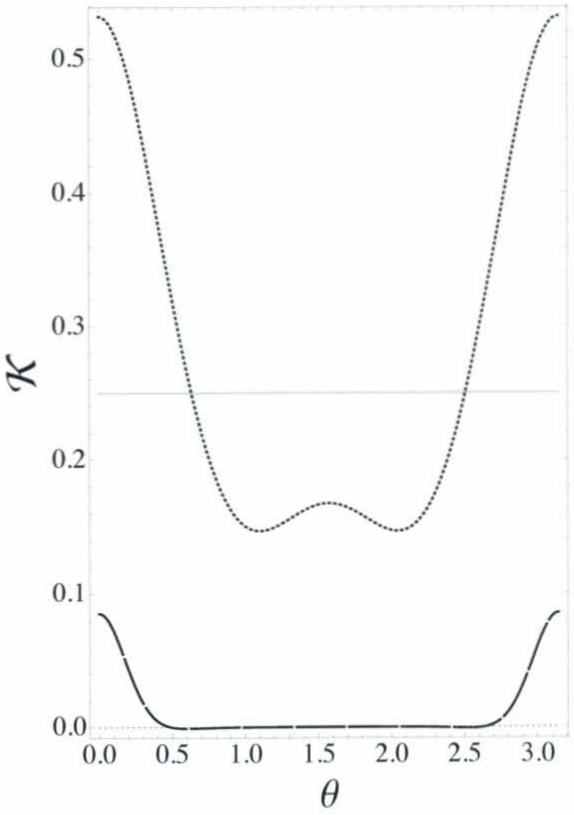

FIGURE 3.7. Gaussian curvature of the horizon for a hexadecapole distortion for $\alpha_4 = 0$, $-\frac{1}{10}$ and -2.37.

3.5.3. External Dipole-Octupole Field. Though we cannot have individual odd multipole distortions, we can have combinations, since the requirement (Equation 2.9) is that the sum of odd multipoles must be zero. Consider a dipole-octupole

distortion. Then

$$\sum_{k=1}^{\infty} \alpha_{2k-1} \left(\delta_{k1} + \delta_{k2}\right) = \alpha_1 + \alpha_3 = 0 \qquad \Longrightarrow \qquad \alpha = \alpha_1 = -\alpha_3$$

and $u_0 = 0$, so the strong energy condition is satisfied regardless of the value of α. The expansion for a dipole-octupole distortion is given by

$$\Theta_{(n)} = \sin^2\theta \left(1 + 9\cos^4\theta\right) \alpha^2 + 2\left(\cos\theta - 3\cos^3\theta\right) \alpha - 1.$$

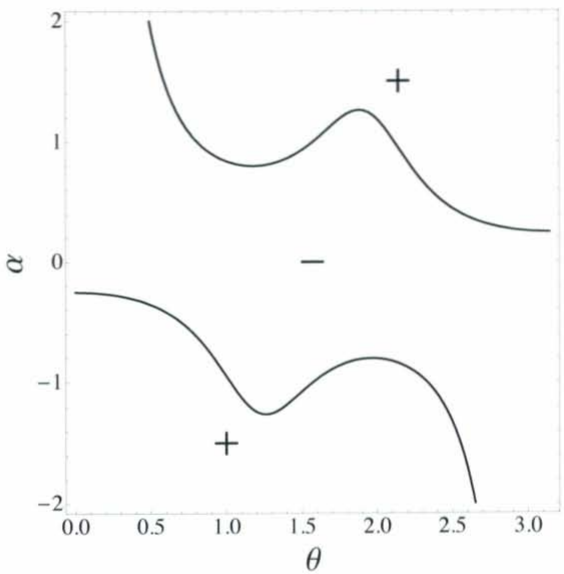

FIGURE 3.8. Graph showing the positive and negative regions of $\Theta_{(n)}$ in a dipole-octupole distortion.

In Figure 3.8 we see that the range for α is bounded between $\pm\frac{1}{4}$ so that $\Theta_{(n)} < 0$ for all values of θ. Thus, in a dipole-octupole distortion with our given foliation, a FOTH is present when the magnitude of the distortion is in the range $-\frac{1}{4} \leq \alpha \leq \frac{1}{4}$.

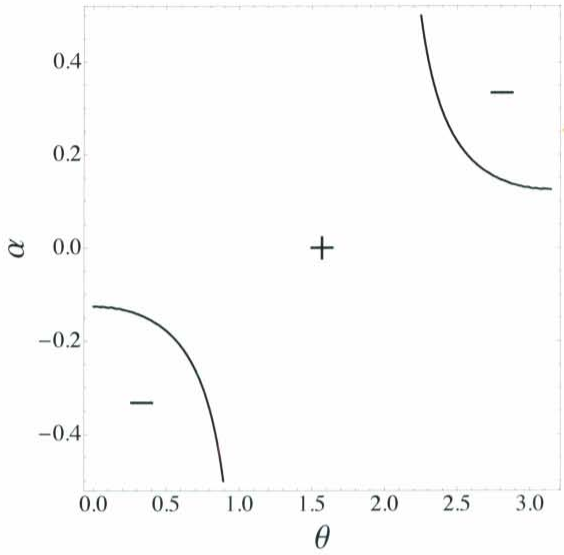

FIGURE 3.9. Graph showing the positive and negative regions of the square of the integrand from Equation 3.13 for a dipole-octupole distortion.

Embedding diagrams are possible for dipole-octupole distortion, with a caveat: not all values of α can be embedded in Euclidean 3-space. The reason for this can be seen in Figure 3.9. This is a graph of the square of the integrand from Equation 3.13,

$$\left(\frac{dz}{d\theta}\right)^2 = 4\mathrm{e}^{\sin\theta\,\sin 2\theta\,\alpha} - \mathrm{e}^{-2\cos\theta\,\sin\theta\,\alpha}\left[\left(1+3\cos^2\theta\right)\sin^2\theta\,\alpha - 2\cos\theta\right]^2.$$

Notice that there are regions where it goes negative, thus the integrand becomes imaginary. Because of this, we are limited to a range of $-0.12 \lesssim \alpha \lesssim 0.12$.

Embedding diagrams for three values of α are shown in Figure 3.10. The grey line shows an undistorted horizon; the dotted line shows $\alpha = -\frac{1}{10}$; and the dashed line shows $\alpha = \frac{1}{10}$. Notice that the behaviour of the negative distortion is opposite to that

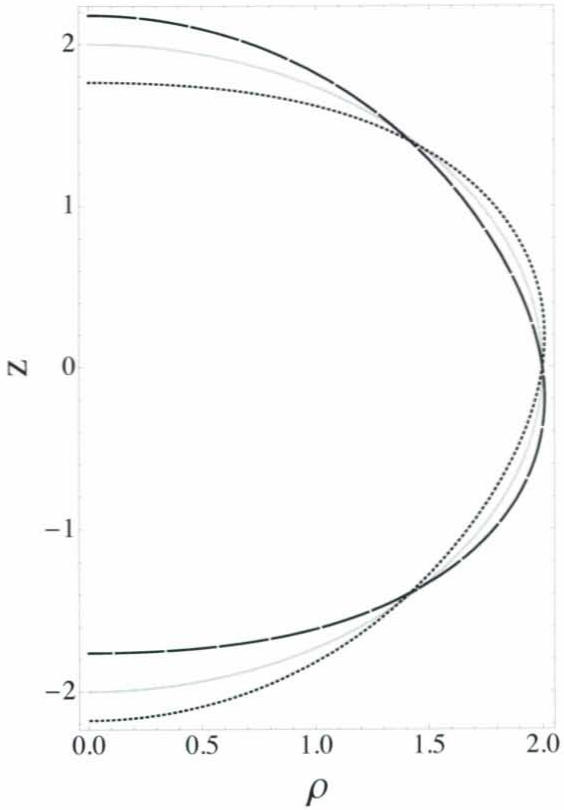

FIGURE 3.10. Embedding diagram for a dipole-octupole distortion for $\alpha = 0$, -0.1 and -0.1.

of the positive distortion. When compared to the undistorted horizon, the positive distortion (dashed line) pulls the horizon away from the north pole, but pushes the horizon inward at the south pole. Alternatively, the negative distortion (dotted line) pulls the horizon away at the south pole and pushes the north pole inward. The

spheroidal geometry is to be expected since, from Figure 3.11, the Gaussian curvature remains positive for $\alpha = -\frac{1}{10}$ (dotted line) and $\alpha = \frac{1}{10}$ (dashed line.)

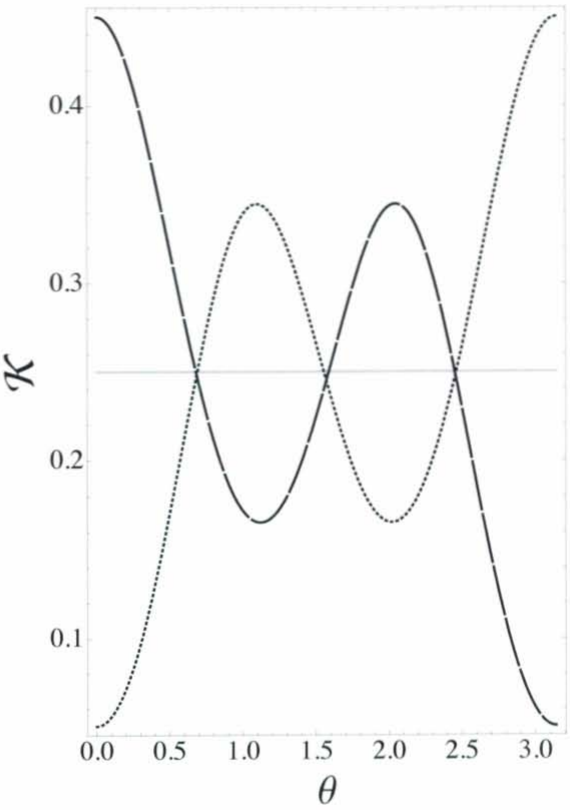

FIGURE 3.11. Gaussian curvature of the horizon for a dipole-octupole distortion for $\alpha = 0$, $-\frac{1}{10}$ and $\frac{1}{10}$.

3.5.4. External Dipole-Quadrupole-Octupole Field. As a final investigation for our chosen foliation, we shall examine a dipole-quadrupole-octupole distortion. Equation 2.9 and Equation 2.10 still hold, so we will have $\alpha = \alpha_1 = -\alpha_3$ and $\alpha_2 \leq 0$. The expansion scalar will be given by

$$\Theta_{(n)} = \mathrm{e}^{2\alpha_2}\Big[\sin^2 2\theta\,\alpha_2^2 + \sin^2\theta\left(1+9\cos^4\theta\right)\alpha^2 + 4\cos^2\theta\,\alpha_2 + 2\cos\theta\left(1-3\cos^2\theta\right)\alpha - 1\Big]. \tag{3.14}$$

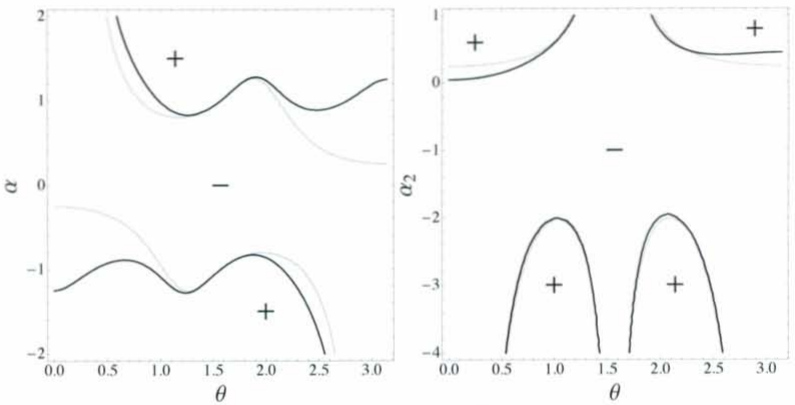

(A) Constant α_2, varying α (B) Constant α, varying α_2

FIGURE 3.12. Comparison of the effects of varying α versus α_2.

We can examine the effects of α and α_2 graphically by plotting Equation 3.14, as in Figure 3.12. Figure 3.12a shows Equation 3.14 for a fixed value of $\alpha_2 = -1$ (the black line) versus the usual dipole-octupole distortion (grey line.) Notice that when the quadrupole field is present, the region where $\Theta_{(n)} < 0$ increases. Figure 3.12b shows Equation 3.14 for a fixed value of $\alpha = -\frac{1}{5}$ (the black line) versus the usual quadrupole

distortion (grey line.) Notice that when the dipole-octupole field is present, the region where $\Theta_{(n)} < 0$ decreases in the northern hemisphere, but increases in the southern hemisphere.

3.6. An Alternate Foliation

We have seen that the standard foliation provides a very limited range of multipole moments for which FOTHs can exist. And, although the foliation chosen in Equation 3.3 provides a great simplification of the expansion scalar, we may wonder if there is an even better foliation; a foliation such that the range of multipole moment magnitudes is increased. As a first attempt, we will consider the following foliation. Let

$$S(\theta) = -m \sin^2\theta + f(2m, \theta). \tag{3.15}$$

Then the expansion scalar, Equation 3.1, becomes

$$\Theta_{(n)} = \frac{1}{m} e^{-6u_0} \left\{ 4e^{4u_0} \left[\sum_{i=1}^{\infty} \left(2\,i \cos^i\theta\, \alpha_i + i^2 \sin^2\theta \cos^{2(i-1)}\theta\, \alpha_i^2 \right) - 1 \right] \right.$$
$$\left. - e^{2u_0} (1 + 3\cos 2\theta) + \cos^2\theta \sin^2\theta \right\}. \tag{3.16}$$

We see that we get back the expansion scalar from Equation 3.5—as expected from the presence of a $f(2m, \theta)$ term in our new foliation—along with two additional terms arising from the $-m \sin^2\theta$ term in the new foliation. Have we achieved a better foliation? As in the previous section, to check this, we will examine the ranges of the multipole moment magnitudes.

From Figure 3.13a, the range of α_2 is now $-2 \leq \alpha_2 < 0.34$. Recall that the range of the previous foliation, Equation 3.3, for a quadrupole distortion was $-2 \leq \alpha_2 \leq 0.25$. Thus, the range of a quadrupole distortion in this new foliation is better than that

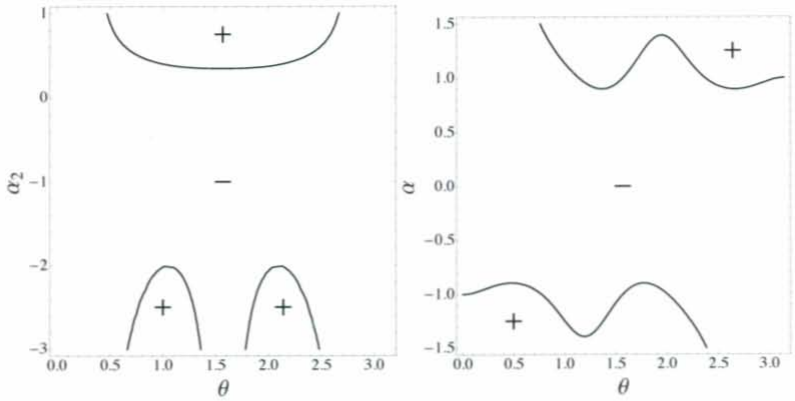

(A) Expansion for quadrupolar distortion with the alternate foliation.

(B) Expansion for dipoctupolar distortion with the alternate foliation.

FIGURE 3.13. Expansion scalars for the alternate foliation.

in Equation 3.3. From Figure 3.13b, the range of α is now $-0.89 < \alpha < 0.89$ as compared to the original range of $-0.25 \leq \alpha \leq 0.25$. Thus, the range of a dipole-octupole distortion is also increased. The embedding diagrams will be unchanged, since they do not depend on the foliation.

3.7. A Generic Foliation

Since the range of multipole moment magnitudes is improved by the foliation given in Equation 3.15, we may wonder if even better foliations exist that keeps $\Theta_{(n)} < 0$ regardless of the values of the α_i. As mentioned in section 3.3, the complexity of the expansion scalar limits the likelihood of such a foliation. We will use the following argument to show that in general there is no foliation that will make $\Theta_{(n)} < 0$. We will, however, be able to bound the range of quadrupole distortions and, by extension,

other distortions. First, we shall set

$$S(\theta) = h(\theta) + f(2m, \theta)$$

where h will be the function that would admit an always negative expansion. The presence of f is to avoid the positive regions as in section 3.2. Furthermore, we will concentrate on a quadrupole distortion—if we can show that h diverges for even the quadrupole, then $\Theta_{(n)}$ will diverge in general. Then the expansion scalar will be

$$\Theta_{(n)} = \frac{1}{4m^2} e^{4\alpha_2} \frac{d^2h}{d\theta^2} + \frac{1}{16m^3} e^{6\alpha_2} \left(\frac{dh}{d\theta}\right)^2 + \frac{1}{4m^2} e^{4\alpha_2} \cot\theta \frac{dh}{d\theta} + \frac{1}{m} e^{2u_0} \Big(4\cos^2\theta \, \sin^2\theta \, \alpha_2^2 + 4\cos^2\theta \, \alpha_2 - 1\Big).$$

To simplify this expression, we can scale the metric such that $2m = e^{2\alpha_2}$. Recalling the strong energy condition, we make the substitution $\alpha_2 = -a$ where $a \geq 0$. Then we get

$$\Theta_{(n)} = \frac{d^2h}{d\theta^2} + \frac{1}{2}\left(\frac{dh}{d\theta}\right)^2 + \cot\theta \frac{dh}{d\theta} + 2\Big(4\cos^2\theta \, \sin^2\theta \, a^2 - 4\cos^2\theta \, a - 1\Big).$$

Notice that there are still problems with this expansion at the poles. To avoid this, we work from the equator by making the substitution $\theta = \frac{\pi}{2} + x$, where $-\frac{\pi}{2} \leq x \leq \frac{\pi}{2}$ and the equator occurs at $x = 0$. Finally, we will make the substitution $\frac{dh}{d\theta} = -\lambda$. We will then have

$$\Theta_{(n)} = -\frac{d\lambda}{dx} + \frac{1}{2}\Big(\lambda + \tan x\Big)^2 - \frac{1}{2}\tan^2 x + 2\Big(4\cos^2 x \, \sin^2 x \, a^2 - 4\sin^2 x \, a - 1\Big).$$

Since we are concerned whether the expansion is positive or negative, we must have

$$\frac{d\lambda}{dx} > \frac{1}{2}\Big(\lambda + \tan x\Big)^2 - \frac{1}{2}\tan^2 x + 2\Big(4\cos^2 x \, \sin^2 x \, a^2 - 4\sin^2 x \, a - 1\Big).$$

The question then becomes: can we find such a λ? The first part is clearly greater than zero, so we need

$$\frac{d\lambda}{dx} > -\frac{1}{2}\tan^2 x + 2\Big(4\cos^2 x \sin^2 x\, a^2 - 4\sin^2 x\, a - 1\Big). \tag{3.17}$$

If we integrate both sides, we get

$$\lambda(x) > \lambda(0) + \int_0^x \left[-\frac{1}{2}\tan^2 x' + 2\Big(4\cos^2 x' \sin^2 x'\, a^2 - 4\sin^2 x'\, a - 1\Big)\right] dx'.$$

However, $\lambda(0) = h'\left(\frac{\pi}{2}\right) = 0$ due to the symmetry of the horizon. So

$$\lambda(x) > \left(x - \frac{1}{4}\sin 4x\right) a^2 + 2\left(\sin 2x - 2x\right) a - \frac{1}{2}\left(3x + \tan x\right). \tag{3.18}$$

We fix $x = \frac{\pi}{6}$. Then Equation 3.18 becomes

$$\lambda\left(\frac{\pi}{6}\right) > 0.31a^2 - 0.36a - 1.07 \tag{3.19}$$

which has a zero at $a \approx 2.6$, so we fix $a = 4$ to bound λ; to pick a region where λ is positive. Then $\lambda\left(\frac{\pi}{6}\right) > 2.39$. Furthermore, for $a = 4$, Equation 3.17 is greater than zero on the range $0.15 \lesssim x \lesssim 1.01$ (i.e. $1.7 \lesssim \theta \lesssim 2.6$), which means $\lambda'(x) > 0$ on the range $\frac{\pi}{6} \approx 0.52 \lesssim x \lesssim 1.01$. Because of this, $\lambda(x) > 0$ on this same range, since it began positive and is increasing on the range. Thus, we must also have

$$\frac{d\lambda}{dx} > \frac{1}{2}\Big(\lambda + \tan x\Big)^2 > \frac{1}{2}\lambda^2$$

on this range. It seems obvious that this will diverge, and so h' and h'' will also diverge. If we let $\lambda = \lambda_0 + \Lambda$ where $\lambda_0' = \frac{1}{2}\lambda_0^2$ with $\lambda_0\left(\frac{\pi}{6}\right) = 2$ and $\Lambda\left(\frac{\pi}{6}\right) > 0.39$.

Then

$$\lambda' > \frac{1}{2}\lambda^2$$
$$\lambda_0' + \Lambda' > \frac{1}{2}\lambda_0^2 + \lambda_0\Lambda + \frac{1}{2}\Lambda^2$$
$$\Lambda' > \lambda_0\Lambda + \frac{1}{2}\Lambda^2 > \lambda_0\Lambda.$$

And so, if $\Lambda > 0$ and λ_0 diverges, then Λ must diverge. We solve $\lambda_0' = \frac{1}{2}\lambda_0^2$ for λ_0 to get

$$\lambda_0(x) = \frac{2}{1 - \left(x - \frac{\pi}{6}\right)}$$

which clearly diverges when $x = 1 + \frac{\pi}{6} < \frac{\pi}{2}$. Now, since λ_0 diverges, Λ will also diverge. So h' and h'' will diverge for $a \gtrsim 4$. Therefore, $\Theta_{(n)}$ will diverge for $\alpha_2 \lesssim -4$.

This lack of a generic solution, what does it mean for our distorted spacetimes and for our local definition of black holes? First, it means that the sort of marginally trapped surfaces for which we have been searching do not exist beyond a certain multipole moment magnitude. We must therefore say that we have reached a limit of the new definition of a black hole as a region of spacetime where a FOTH exists. However, we can turn this around to ask if the failure means that, beyond the limit, the region inside the Schwarzschild radius is even a black hole. In other words, are there no trapped surfaces *at all* inside $r = 2m$? It's a possibility, but the more likely occurrence is that none of the trapped surfaces inside $r = 2m$ are smooth perturbations of a marginally trapped surface (i.e. from a $\Theta_{(\ell)} = 0$ surface). Consider Figure 3.14. We had hoped to find trapped surfaces in the distorted spacetime that looked like Figure 3.14a; surfaces just inside the Schwarzschild radius. What may instead be the case is something more like Figure 3.14b. Rather than the set of

foliating surfaces from Equation 2.6,

$$\Sigma_\sigma = \left\{ (v,\ 2m,\ \theta,\ \phi) \mid v - S(\theta) = \sigma \right\},$$

we may instead have surfaces that look like the example surfaces in Figure 3.14b which would take the form

$$\Sigma_\sigma = \left\{ (v(\theta),\ r(\theta),\ \theta,\ \phi) \mid v(\theta) - S(\theta) = \sigma \right\}. \tag{3.20}$$

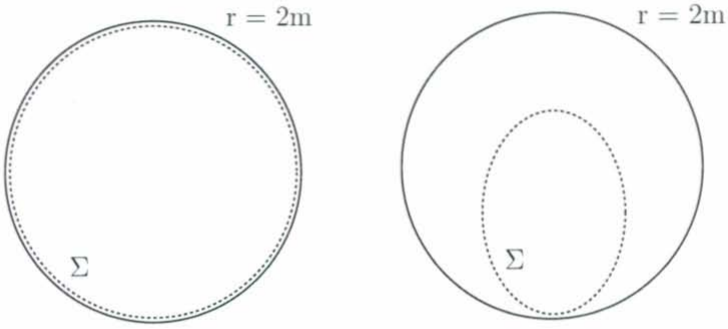

(A) Hoped-for trapped surfaces (dashed line) and the Schwarzschild radius (solid line).

(B) Possible alternative (marginally) trapped surfaces (dashed lines) and the Schwarzschild radius (solid line).

FIGURE 3.14. Possible types of trapped surfaces.

Now, rather than looking only at $r = 2m$ and v =const., we have the radius and time as functions of angle. That means that the trapped surface may stretch forwards or backwards in time as well as space. It seems plausible that these more general

surfaces will provide marginally trapped surfaces for arbitrarily large distortions of the spacetime.

3.8. Concluding Remarks

We began this monograph by asking the question: what is a black hole? Along the way we found two answers to this question. The first was provided by Hawking & Ellis, which states that a black hole is a region of spacetime that cannot be reached from future null infinity along any timelike or null path. The boundary of this region is called the event horizon and we typically say that a spacetime contains a black hole if an event horizon is present.

This definition provides firm footing to describe global properties of a black hole spacetime. However, as we saw, there are problems with the definition arising from the non-local nature of the event horizon. We then introduced the local concept of a future outer trapping horizon to replace the event horizon. A FOTH is described by marginally trapped surfaces such that the outward expansion is zero ($\Theta_{(\ell)} = 0$), the inward expansion is strictly negative ($\Theta_{(n)} < 0$) and the outgoing null geodesics converge just inside the horizon ($\mathcal{L}_n \Theta_{(\ell)} < 0$). So, our question of "what is a black hole" transformed into a question of the existence of a FOTH in the spacetime. We applied the mathematical machinery of trapped surfaces to examine distorted Schwarzschild spacetime. That is, a Schwarzschild black hole placed in an external axisymmetric distribution of matter.

In a global sense, it fails to be a black hole. Since we lose asymptotic flatness (a requirement for the Hawking & Ellis definition), we lose the event horizon and thus the black hole. Are there then no black holes in the presence of external matter distributions? We look at this question instead from a local perspective. We found

two foliations that admitted marginally trapped surfaces and so a FOTH. Using the first of these foliations, we then determined that—when the external field is decomposed into multipole moments—the sum of the odd multipoles must be zero (i.e. no purely dipole distortion, no purely octupole distortion, etc.) and that the sum of the even multipoles must be non-positive. Due to these restrictions, we were able to determine a range of values for a purely quadrupole distortion, a purely hexadecapole distortion and for a dipole-octupole distortion. We then examined the effects of a dipole-quadrupole-octupole distortion, where we determined that the presence of a quadrupole distortion in the midst of a dipole-octupole distortion will serve to increase the range of possible distortion values, but the addition of a dipole-octupole distortion to a quadrupole distortion will decrease the range.

The second foliation we examined improved the range of multipole moment magnitudes which led us to wonder if there was a path to the general solution that eluded us at the beginning. This general foliation, it was hoped, would furnish an expansion that was everywhere negative; that is, regardless of the value of the multipole moments. We found instead that for the quadrupole, there can be no such foliation for $\alpha_2 \lesssim -4$. By extension, there will be a bound on the other moments as well. It may be that the surfaces described in Equation 3.20 could instead be required in the general case, however this is beyond our current formalism.

What then is left to be done in this line of research? We were unable to find a general solution for our foliation, but were able to find two specific foliations that gave FOTHs for some range of multipole moment magnitudes. It would be nice to have a foliation that approaches the limit found in the previous section. Starting from another set of surfaces like Equation 3.20 may even provide the desired everywhere-negative

expansion, though no obvious method seems forthcoming on how to do so. Furthermore, we wonder what manner of matter distributions give rise to values ranges we did find. On a purely technical level, the ranges of higher-order multipole moments and other combinations of multipole moments could be examined. Finally, it would be useful to apply this methodology not only to static (i.e. Schwarzschild) spacetimes, but also to stationary (i.e. Kerr or Kerr-Newman) spacetimes, as they would have more applicability to astrophysical situations than the non-rotating Schwarzschild spacetime. Conceptually this is not a difficult task, though it is computationally daunting.

APPENDIX A

Calculations

A-1. Transformation from Weyl to Schwarzschild

The Weyl metric is given by

$$ds^2 = -e^{2\psi}dt^2 + e^{2(\gamma-\psi)}\left(d\rho^2 + dz^2\right) + e^{-2\psi}\rho^2\, d\phi^2. \tag{A.1}$$

Using the distorted Scwarzschild solutions for ψ and γ,

$$\psi = \frac{1}{2}\ln\left(\frac{r_+ + r_- - 2m}{r_+ + r_- + 2m}\right) + U(\rho, z) \qquad \gamma = \frac{1}{2}\ln\left(\frac{(r_+ + r_-)^2 - 4m^2}{4r_+r_-}\right) + V(\rho, z)$$

where $r_\pm^2 = \rho^2 + (z \pm m)^2$, we get the metric in the form

$$\begin{aligned} ds^2 = &-e^{2U}\left(\frac{r_+ + r_- - 2m}{r_+ + r_- + 2m}\right) dt^2 + e^{2(V-U)}\left(\frac{(r_+ + r_- + 2m)^2}{4r_+r_-}\right)\left(d\rho^2 + dz^2\right) \\ &+ e^{-2U}\left(\frac{r_+ + r_- + 2m}{r_+ + r_- - 2m}\right)\rho^2\, d\phi^2 \end{aligned} \tag{A.2}$$

where $U \equiv U(\rho, z)$ and $V \equiv V(\rho, z)$. Now, starting from Equation A.2, we perform the transformation [**38**]

$$\rho \to \sqrt{r(r-2m)}\,\sin\theta$$

$$z \to (r-m)\cos\theta$$

to obtain the distorted Schwarzschild metric in Schwarzschild coordinates $(t,\ r,\ \theta,\ \phi)$,

$$ds^2 = \mathrm{e}^{2U}\left(1-\frac{2m}{r}\right)dt^2 + \mathrm{e}^{-2U+2V}\left[\frac{dr^2}{1-\frac{2m}{r}} + r^2 d\theta^2\right] + \mathrm{e}^{-2U} r^2 \sin^2\theta d\phi^2 \qquad \text{(A.3)}$$

where U and V are now functions of (r, θ). As usual, in these coordinates, the horizon is at $r = 2m$, where there is also a coordinate singularity. The spacetime singularity is at $r = 0$.

A-2. Transformation from Weyl to Prolate Spheroidal

To obtain the distorted Schwarzschild metric in prolate spheroidal coordinates from the canonical Weyl coordinates, we start from Equation A.2 and perform the transformation [**28**]

$$\rho \to m\sqrt{(x^2-1)\,(1-y^2)}$$

$$z \to mxy.$$

Then, the metric in prolate spheroidal coordinates $(t,\ x,\ y,\ \phi)$ is given by

$$ds^2 = -\mathrm{e}^{2U}\frac{x-1}{x+1}dt^2 + \mathrm{e}^{2(V-U)}m^2\left[\frac{x+1}{x-1}dx^2 + \frac{(x+1)^2}{1-y^2}dy^2\right]$$
$$+ \mathrm{e}^{-2U}m^2(x+1)^2(1-y^2)d\phi^2 \qquad \text{(A.4)}$$

where U and V are now functions of (x, y). In these coordinates, the horizon is at $x = 1$ and $-1 \leq y \leq 1$. There are coordinate singularities at $x = 1$, $y = -1$ and $y = 1$. The spacetime singularity is at $x = -1$.

A-3. Transformation from Prolate Spheroidal to Schwarzschild

We start from Equation A.4 and performing the transformation [**39**]

$$x \to \frac{r}{m} - 1$$
$$y \to \cos\theta.$$

We obtain the distorted Schwarzschild metric in Schwarzschild coordinates $(t,\ r,\ \theta,\ \phi)$,

$$ds^2 = \mathrm{e}^{2U}\left(1 - \frac{2m}{r}\right)dt^2 + \mathrm{e}^{-2U+2V}\left[\frac{dr^2}{1-\frac{2m}{r}} + r^2 d\theta^2\right] + \mathrm{e}^{-2U} r^2 \sin^2\theta d\phi^2$$

where U and V are now functions of (r, θ).

A-4. Metric Transformation Function

In section 2.1, we explicitly defined the transformation of the time coordinate as

$$t \to v - f(r,\theta) \tag{A.5}$$

where

$$f(r,\theta) = \int_{r_0}^{r} \frac{\mathrm{e}^{-2U(r',\theta)+V(r',\theta)}}{1-\frac{2m}{r'}}\, dr'.$$

We may wonder why this sort of transformation is applicable. First, consider the exterior derivative of Equation A.5,

$$dt = dv - \frac{\partial f}{\partial r}\, dr - \frac{\partial f}{\partial \theta}\, d\theta.$$

Now, we know (see, e.g. [**40**]) that $d(d\alpha) = 0$ for any α. So, we should have $d(dt) = 0$. Furthermore, we also have $dx \wedge dx = 0$ and $dy \wedge dx = -dx \wedge dy$ for any x, y and $df = \frac{\partial f}{\partial x^i} dx^i$ for any function $f(x_1, x_2, \ldots, x_n)$. Taking the exterior derivative

again, we get

$$\begin{aligned} 0 = d(dt) &= d(dv) - d\left(\frac{\partial f}{\partial r}\, dr\right) - d\left(\frac{\partial f}{\partial \theta}\, d\theta\right) \\ &= -\frac{\partial^2 f}{\partial r^2}\, dr \wedge dr - \frac{\partial^2 f}{\partial \theta \partial r}\, d\theta \wedge dr - \frac{\partial^2 f}{\partial r \partial \theta}\, dr \wedge d\theta - \frac{\partial^2 f}{\partial \theta^2}\, d\theta \wedge d\theta \\ &= \left(\frac{\partial^2 f}{\partial r \partial \theta} - \frac{\partial^2 f}{\partial \theta \partial r}\right) dr \wedge d\theta. \end{aligned}$$

Since partial derivatives commute, this is indeed zero and transformations of the sort in Equation A.5 are valid coordinate transformations.

Bibliography

[1] J. Michell, "On the means of discovering the distance, magnitude, &c. of the fixed stars, in consequence of the diminution of the velocity of their light, in case such a diminution should be found to take place in any of them, and such other data should be procured from observations, as would be farther necessary for that purpose," *Philosophical Transactions of the Royal Society of London* **74** (1784) 35.

[2] W. Israel, "Dark stars: the evolution of an idea," in *300 Years of Gravitation*, S. Hawking and W. Israel, eds. Cambridge UP, 1987.

[3] K. S. Thorne, *Black Holes and Time Warps*. W. W. Norton, 1994.

[4] R. M. Wald, *General Relativity*. University of Chicago Press, 1984.

[5] E. Poisson, *A Relativist's Toolkit*. Cambridge UP, 2004.

[6] K. Schwarzschild, "On the gravitational field of a sphere of incompressible fluid according to einstein's theory," *Sitzungsberichte der Königlich Preussischen Akademie der Wissenschaften zu Berlin, Phys.-Math. Klasse* (1916) 424, `arXiv:physics/9912033`. Translation by S. Antoci.

[7] J. R. Oppenheimer and H. Snyder, "On continued gravitational collapse," *Physical Review* **56** (1939) 455.

[8] J. Wheeler and K. Ford, *Geons, Black Holes and Quantum Foam*. W. W. Norton, 1998.

[9] R. Penrose, "Gravitational collapse and space-time singularities," *Physical Review Letters* **14** (1965) no. 3, 57.

[10] S. Hawking and G. Ellis, *The Large Scale Structure of Space-Time*. Cambridge UP, 1973.

[11] S. Hayward, "Black holes: new horizons," in *Ninth Marcel Grossmann Meeting*, V. Gurzadyan, R. Jantzen, and R. Ruffini, eds., p. 568. World Scientific Publishing, Singapore, 2000. `arXiv:gr-qc/0008071v2`.

[12] A. Ashtekar and B. Krishnan, "Isolated and dynamical horizons and their applications," *Living Reviews in Relativity* **7** (2004) no. 10, . http://www.livingreviews.org/lrr-2004-10.

[13] I. Booth, "Black hole boundaries," *Canadian Journal of Physics* **83** (2005) no. 11, 1073, arXiv:gr-qc/0508107v2.

[14] P. Hájiček, "Exact models of charged black holes: I. geometry of totally geodesic null hypersurface," *Communications in Mathematical Physics* **34** (1973) 37.

[15] S. Hayward, "General laws of black-hole dynamics," *Physical Review D* **49** (1994) no. 12, 6467, arXiv:gr-qc/9303006v3.

[16] A. Ashtekar, C. Beetle, and S. Fairhurst, "Isolated horizons: A generalization of black hole mechanics," *Classical and Quantum Gravity* **16** (1999) no. 2, L1, arXiv:gr-qc/9812065.

[17] R. Sachs, "Graviatational waves in general relativity. vi. the outgoing radiation condition," *Proceedings of the Royal Society of London. Series A, Mathematical and Physical Sciences* (1961) no. 264, 309.

[18] P. Chruściel, G. Galloway, and D. Pollack, "Mathematical general relativity: a sampler," *Bulletin of the american mathematical society* **47** (2010) no. 4, 567, arXiv:1004.1016.

[19] S. Chandrasekhar, *The Mathematical Theory of Black Holes*. No. 69 in International Series of Monographs on Physics. Oxford UP, 1983.

[20] T. Regge and J. A. Wheeler, "Stability of a schwarzschild singularity," *Physical Review* **108** (1957) no. 4, 1063.

[21] F. J. Zerilli, "Effective potential for even-parity regge-wheeler gravitational perturbation equations," *Physical Review Letters* **24** (1970) no. 13, 737.

[22] C. V. Vishveshwara, "Stability of the schwarzschild metric," *Physical Review D* **1** (1970) no. 10, 2870.

[23] K. Martel and E. Poisson, "Gravitational perturbations of the schwarzschild spacetime: a practical covariant and gauge-invariant formalism," *Physical Review D* **71** (2005) 104003, arXiv:gr-qc/0502028.

[24] L. Mysak and G. Szekeres, "Behavior of the schwarzschild singularity in superimposed gravitational fields," *Canadian Journal of Physics* **44** (1966) .

[25] W. Israel and K. Khan, "Collinear particles and bondi dipoles in general relativity," *Il Nuovo Cimento* **33** (1964) no. 2, 331.

[26] A. Doroshkevich, Y. Zel'dovich, and I. Novikov, "Gravitational collapse of nonsymmetric and rotating masses," *Soviet Physics JETP* **22** (1965) no. 1, 122.

[27] W. Israel, "Entropy and black-hole dynamics," *Lettere Al Nuovo Cimento* **6** (1973) no. 7, 267.

[28] N. Bretón, T. Denisova, and V. Manko, "A kerr black hole in the external gravitational field," *Physics Letters A* **230** (1997) 7.

[29] S. Fairhurst and B. Krishnan, "Distorted black holes with charge," *International Journal of Modern Physics D* **10** (2001) no. 5, 691, `arXiv:gr-qc/0010088`.

[30] J. Fitgerald, "Exterior geodesics in distorted schwarzschild spacetimes." B.Sc. thesis - Memorial University of Newfoundland, 2008.

[31] R. Geroch and J. Hartle, "Distorted black holes," *Journal of Mathematical Physics* **23** (1982) no. 4, 680.

[32] E. Kreyszig, *Introduction to Differential Geometry and Riemannian Geometry.* University of Toronto Press, 1968.

[33] R. Geroch, "Multipole moments ii: Curved space," *Journal of Mathematical Physics* **11** (1970) no. 8, 2580.

[34] R. Hansen, "Multipole moments of stationary space-times," *Journal of Mathematical Physics* **15** (1974) no. 1, 46.

[35] K. S. Thorne, "Multipole expansions of gravitational radiation," *Reviews of Modern Physics* **52** (1980) no. 2, 299.

[36] D. Zwillinger, *Handbook of Differential Equations.* Academic Press, 3 ed., 1998.

[37] I. Booth and S. Fairhurst, "Extremality conditions for isolated and dynamical horizons," *Physical Review D* **77** (2008) 084005, `arXiv:0708.2209`.

[38] W.-M. Suen, "Distorted black holes in terms of multipole moments," *Physical Review D* **34** (1986) no. 12, 3633.

[39] H. Quevedo, "General static axisymmetric solution of einstein's vacuum field equations in prolate spheroidal coordinates," *Physical Review D* **39** (1989) no. 10, 2904.

[40] B. Schutz, *Geometrical Methods of Mathematical Physics.* Cambridge UP, 1980.